Thermal Characterisation and Modelling for a Single Sided Axial Flux SMC Stator

James Keogh and Salman Babar

MASTER'S THESIS
Electromechanical Vehicle Engineering
Department of Engineering Science

June 18th 2025

MASTER'S THESIS

Thermal Characterisation and Modelling for a Single Sided Axial Flux SMC Stator

Abstract

This study investigates the thermal behaviour of a single-sided axial flux electric motor stator composed of a soft magnetic composite (SMC) material through experimental characterization and lumped parameter thermal modelling. With increasing demands for compact and high-power-density motor designs, effective thermal management becomes critical to ensure reliability and performance. The research focuses on both DC and AC loading conditions, employing a spatially resolved sensor network to capture detailed temperature distributions across stator components such as windings, yoke, and teeth. A two-stage modelling approach was implemented: an initial single-node thermal network validated basic assumptions, followed by a refined multi-node model capable of simulating transient and spatial thermal behaviour with high fidelity. Experimentally determined thermal conductivities and convection coefficients, alongside a tailored nodal network, enabled the accurate prediction of temperature evolution. Validation against experimental data showed a maximum absolute error of under 10 °C, with coil temperature predictions consistently within 5 °C. The model successfully incorporated AC iron losses using the Steinmetz equation, demonstrating applicability to dynamic operating scenarios. This work establishes a validated, adaptable methodology for thermal analysis of axial flux electric machine stators, supporting future design optimization and thermal management strategies.

Date:	April 28, 2025
Author(s):	Salman Babar, James Keogh
Examiner:	Lars Bergqvist
Advisor(s):	Danyang Cui (University West), Pontus Fyhr (Alvier Mechatronics AB)
Programme name:	Electromechanical Vehicle Engineering
Main field of study:	Engineering
Course credits:	15 HE credits
Publisher:	University West, Department of Engineering Science, S-461 86 Trollhättan, SWEDEN

Contents

1 Introduction **4**

2 Literature Review **6**

3 Theoretical Background **10**
3.1 Functional Principles 10

4 First Iteration Model **13**
4.1 First Iteration Methodology 13
4.2 First Iteration Experimental Setup 16
4.3 First Iteration Results 17
4.4 First Iteration Discussion 19

5 Second Iteration Model **21**
5.1 Second Iteration Methodology 21
5.2 Second Iteration Experimental Setup 27
5.3 Second Iteration Results 31
5.3.1 Determining Heat Transfer Coefficients Results 31
5.3.2 Total Nodal Network Results 34
5.4 Second Iteration Discussion 42

6 Conclusion **45**

7 References **46**

List of Figures:

Figure 1: Drawing of geometric simplification *12*
Figure 2: 3-D Geometric simplification of the coil *12*
Figure 3: Illustration of 1st iteration simplification *13*
Figure 4: Basic thermal circuit representation *15*
Figure 5: Coil on stator, DC experimental setup *16*
Figure 6: First iteration temperature evolution *17*
Figure 7: First iteration temperature evolution with curve fitting *18*
Figure 8: First iteration error *18*
Figure 9: Measured electrical data *19*
Figure 10: 3-D Render of coil on stator *23*
Figure 11: Geometric segmentation of system *24*
Figure 12: Analogous electrical circuit of coil on stator *24*
Figure 13: Overlay of the electrical circuit on the stator teeth *25*
Figure 14: Determining the h value experimental setup *28*
Figure 15: Determining k values experimental setup *29*
Figure 16: AC experimental setup side view *30*
Figure 17: AC experimental setup top view *30*
Figure 18: Experimental data for evaluation of k *31*
Figure 19: Experimental k value results *32*
Figure 20: Experimental h value method 1 ..... *33*
Figure 21: Experimental h value method 2 ..... *33*
Figure 22: Simulation results for 10A DC, Run 1 ..... *35*
Figure 23: Errors for 10A DC, Run 1 ..... *35*
Figure 24: Simulation results for 15A DC, Run 1 ..... *36*
Figure 25: Errors for 15A DC, Run 1 ..... *36*
Figure 26: Simulation results for 10A DC, Run 2 ..... *37*
Figure 27: Errors for 10A DC, Run 2 ..... *37*
Figure 28: Simulation results for 15A DC, Run 2 ..... *38*
Figure 29: Errors for 15A DC, Run 2 ..... *38*
Figure 30: AC test results with DC simulation *39*
Figure 31: AC tested and DC simulated errors *40*
Figure 32: AC test results with AC simulation *40*
Figure 33: AC tested and simulated errors *41*

List of Tables:

Table 1: Experimentally determined values for the Steinmetz equation *27*

Nomenclature

Glossary

LPTN	Lumped Parameter Thermal Network
LPTM	Lumped Parameter Thermal Model
FEA	Finite Element Analysis
SMC	Soft Magnetic Composite
CFD	Computational Fluid Dynamics
AFPM	Axial Flux Permanent Magnet
AFPMSM	Axial Flux Permanent Magnet Synchronous Machine
TEFC	Totally Enclosed Fan Cooled
PMSM	Permanent Magnet Synchronous Machine
BEV	Battery Electric Vehicle
AC	Alternating Current
DC	Direct Current
RMS	Root Mean Squared

Symbols

$\boldsymbol{P_d}$	Dissipated Power in W
$\boldsymbol{P_{Fe}}$	Iron Losses in $\frac{W}{kg}$
$\boldsymbol{R_{el}}$	Electrical Resistance in Ω
$\boldsymbol{C_{th}}$	Thermal Capacitance in $\frac{J}{K}$
$\boldsymbol{R_{th}}$	Thermal Resistance in $\frac{K}{W}$
$\boldsymbol{G}$	Thermal Conductance in $\frac{W}{K}$
$\boldsymbol{k}$	Conductive Heat Transfer Coefficient in $\frac{W}{mK}$
$\boldsymbol{h}$	Convective Heat Transfer Coefficient in $\frac{W}{m^2K}$
$\boldsymbol{\dot{Q}}$	Heat Rate in $\frac{W}{s}$

1 Introduction

The thermal performance of electric motors is vital for their reliability, efficiency, and longevity. Electric motors are critical components across a wide range of applications, from industrial systems to electric vehicles **[1].** Among them, axial-flux permanent magnet (AFPM) motors are a very attractive choice for high-power density applications where space and weight are critical **[2].** However, higher power density and compact packaging inevitably lead to greater heat generation, making thermal management an even bigger challenge **[30].** Effectively managing this heat is fundamental to ensuring motor performance and extending operational lifespans **[3].**

With higher power density and compact packaging leading to greater heat generation, one of the key challenges becomes effectively characterising the thermal behaviour of the machine. Thermal models are typically used to predict and analyse the heat distribution and flow within the motor. By accurately characterising thermal behaviour, these models provide insights that allow for better design optimization, efficient heat dissipation strategies, and safer operation, ultimately ensuring longer motor lifespans and reliable performance **[1] [2]**.

Several thermal modelling techniques are employed to characterise and predict the thermal performance of electric motors, each offering unique advantages and trade-offs. For high-fidelity thermal analysis, Computational Fluid Dynamics (CFD) and Finite Element Analysis (FEA) are often used. These methods capture detailed heat transfer, conduction, and fluid flow phenomena, providing an accurate representation of thermal behaviour. However, they tend to be computationally expensive and require significant modelling expertise, which can limit their application in real-time or large-scale simulations **[4] [6].**

In contrast, Lumped Parameter Thermal Networks (LPTNs) offer a simplified yet effective approach by modelling the system as a network of thermal resistances and capacitances. This method is computationally faster and better suited for system-level studies and transient simulations, such as evaluating drive cycles in electric vehicles. While less detailed than CFD or FEA, LPTNs strike a balance between accuracy and efficiency, making them valuable for evaluating overall system performance in a practical and scalable manner **[4].**

A lumped parameter thermal networks (LPTNs), simplifies the motor's complex thermal behaviour into manageable resistances and capacitances **[5].** While effective, the accuracy of such models hinges on experimental validation and detailed knowledge of material properties and internal heat paths. Several studies have been published concerning the thermal analysis and modelling of electric motors using LPTNs **[7] [11].** Lumped parameter thermal models have been proposed with varying degrees of complexity, with comparisons against

experimental measurements typically limited to a few steady-state or transient operating points **[9].** Investigations often focus on high-level thermal behaviour under standardized conditions, providing valuable but sometimes limited insight into more dynamic operating scenarios **[8].**

In many cases, experimental validation is performed with limited sensor placements, which restricts the ability to capture spatial temperature variations across critical motor regions such as the windings, yoke, and stator teeth **[10] [12].** Furthermore, thermal responses to AC loads at frequencies affecting skin effects and localised heating remain under-explored in the literature, despite their increasing relevance in high frequency switching environments.

Additionally, while data-driven thermal modelling is gaining traction, relatively few studies provide transparent methodologies for parameter identification, model validation, and subsequent design optimization. This lack of traceable and detailed experimental backing limits the broader applicability of many published models, particularly when considering specific design improvements for stator configurations or cooling strategies **[11].**

Thus, there remains a clear need for studies that:

- Combine comprehensive experimental thermal testing across DC and AC loads.
- Offer spatially resolved temperature data within the stator structure.
- Build validated, detailed thermal models capable of supporting design optimization efforts.

The purpose of this thesis is to experimentally investigate and model the thermal behaviour of an electric motor stator, with the goal of supporting design optimisation through improved thermal management. Special emphasis is placed on capturing the effects of both DC and AC currents at varying frequencies, and on developing a validated lumped parameter thermal model based on experimentally identified parameters.

The main contributions of this work are:

- Experimental thermal characterisation of a stator and winding under controlled DC and AC loading.
- Deployment of a spatially resolved temperature sensing setup, enabling detailed measurement across windings, yoke, and stator teeth.
- Development and validation of a lumped parameter thermal model, incorporating thermal resistances and capacitances identified from real-world test data.
- Establishment of a methodology for steady-state and transient thermal analysis to support future electric motor design optimisations.

2 Literature Review

Electric motors convert electrical energy into mechanical energy, but not all of it becomes useful work — some is lost as heat. The amount of heat lost depends on the motor's operating conditions, including the load level, input current, supply frequency (AC), and ambient temperature. Higher loads and frequencies increase losses, raising internal temperatures.

As components like windings, insulation, and the core heat up, excessive temperatures can lead to insulation breakdown, increased copper resistance (which generates even more heat), weakened permanent magnets, and mechanical stress from thermal expansion. These effects reduce the electric motor's efficiency, shorten lifespan, and may even result in sudden failure.

Thermal performance is a measure of how well the motor handles this heating and stays within safe temperature limits under varying operating conditions.

Assessing the thermal performance of an electric motor begins with the thermal characterization of its key components — which in our case is the stator, and the winding. Thermal characterization involves determining how heat is generated, distributed, and dissipated within the stator across different electrical inputs, using experimental testing and thermal modelling.

Experimental testing provides temperature-time data at locations such as the windings, yoke, and stator teeth, under controlled input conditions. These measurements capture how the stator responds thermally to varying currents and frequencies. Thermal modelling complements this by abstracting the physical system into a network of thermal resistances and capacitances, allowing the heat transfer behaviour to be predicted and analysed systematically. Identifying key thermal properties is critical to ensuring model accuracy and enabling targeted design improvements.

Together, testing and modelling form a complete thermal characterization framework. This enables engineers to understand spatial and temporal temperature gradients, identify dominant heat flow paths, and quantify the thermal response at a component level. Such characterization is fundamental for evaluating thermal performance, comparing design alternatives, and guiding thermal management strategies (cooling).

With this background, the remaining section reviews relevant literature on the thermal aspects of electric machines, setting the context of our thesis study.

Understanding the thermal behaviour of electric motors requires a strong grasp of fundamental heat transfer principles. The behaviour of heat within motor components—how it is generated, conducted, convected, and radiated—is

governed by classical heat transfer theory. Foundational texts such as Fundamentals of Heat and Mass Transfer **[13],** A Heat Transfer Textbook **[14],** and Heat Transfer **[15]** provide a comprehensive basis for this understanding, as well as describe the essential boundary and transient conditions critical for analysing dynamic temperature behaviour. These foundational works inform both analytical and numerical thermal models.

Building on the principles of heat transfer, thermal modelling provides a practical framework for simulating the heat flow and temperature distribution within electric machines. Among the various modelling approaches, lumped parameter thermal models (LPTMs) have become particularly prominent due to their balance between computational efficiency and modelling fidelity. These models represent the physical structure of a machine using an analogous thermal network composed of nodes, each of which has a given temperature and is connected by thermal resistances and capacitances. Each component of the motor—such as the stator yoke, windings, and teeth—is abstracted into discrete elements with assigned thermal properties, enabling time-resolved analysis of heat flow and temperature rise under different operating conditions. Gerling and Dajaku **[16]**, critically evaluates the accuracy of traditional lumped-parameter approaches when applied to systems with distributed heat generation, like stator windings. They propose a refined approach that distributes heat input more realistically, either by applying half the losses to a central node or dynamically adjusting node placement to the location of peak temperature.

While LPTMs offer a computationally efficient framework for simulating temperature rise in electric machines, their effectiveness depends heavily on the geometry and operating specifics of the machine under study. In this context, axial-flux permanent-magnet synchronous motors (AFPMSMs) present unique thermal challenges due to their distinctive geometry, compact structure, and typically high-power densities. Shazly et al. **[17]** provide a comprehensive review of the thermal modelling landscape for AFPMSMs. Their work brings attention the fact that, despite the growing adoption of AFPMSMs in space-constrained applications such as electric vehicles and aerospace systems, thermal modelling for these machines has not been as extensively explored as for radial flux counterparts. The review classifies existing thermal modelling approaches—ranging from lumped parameter methods to finite element analysis (FEA) and computational fluid dynamics (CFD)—and evaluates them based on their accuracy, computational demands, and applicability to different AFPMSM configurations.

Shazly et al. **[17]** emphasize that LPTMs remain a popular choice for AFPMSMs due to their ability to capture transient thermal behaviour with relatively low computational cost. However, the authors also point out the limitations of LPTMs in representing non-uniform heat generation and complex geometries, especially in

machines with high aspect ratio components such as the stator and winding of single-sided AFPMSMs. Advanced techniques like FEA and CFD offer higher spatial resolution and can incorporate detailed material properties and cooling effects, but they are often impractical for iterative design due to their resource intensity. The review also identifies the lack of recent experimental validation studies as a key limitation in the literature, stressing the need for more empirical data to support and calibrate thermal models, particularly under realistic loading and cooling conditions.

A cornerstone in the development of lumped parameter thermal models (LPTMs) for electric machines is the work of Mellor, Roberts, and Turner **[18]**, who introduced a comprehensive and experimentally validated LPTM tailored for Totally Enclosed Fan Cooled (TEFC) induction motors. Their model, notable for its simplicity and adaptability, was formulated using only dimensional data and constant thermal coefficients, making it broadly applicable across different motor sizes and configurations. By reducing the thermal behaviour of a TEFC motor to eight linear differential equations, the authors achieved a rare balance between model fidelity and computational efficiency, enabling applications in real-time thermal monitoring and duty-cycle evaluation. This study remains highly influential because it systematically decomposes the motor into thermally relevant subcomponents, capturing key conduction and convection paths, and providing a template for subsequent modelling efforts across machine types.

The limitations in conventional LPTMs when applied to asymmetric geometries, identified by Shazly et al. **[17]** are directly addressed by Nordlund et al. **[19]**, adapting LPTMs to axial-flux geometries using a layered discretization scheme to better represent radial and axial heat flows. Their model, validated experimentally under varying load and cooling conditions, demonstrated the feasibility of extending LPTMs to more complex machines.

In contrast to simplified lumped-parameter models, Marignetti and Delli Colli **[20]** employed coupled thermal and fluid dynamic finite-element analysis (FEA) to investigate the temperature distribution within an axial flux permanent-magnet synchronous machine (AFPMSM) constructed using soft magnetic composite (SMC) material. Their study emphasizes the critical role of accurate convection modelling in axial flux machines, where conventional assumptions used in radial machines often fall short due to distinct geometric and cooling characteristics. Especially their comparative study between rectified and axisymmetric models revealed the limitations of oversimplified approaches and reinforced the need for geometry-aware modelling—especially in SMC-based AFPMSMs.

While many modelling efforts show promise, a key limitation in the field is the scarcity of experimental validation under realistic operating conditions. Shazly et al. **[17]** and Nordlund et al. **[19]** both note this deficit, calling for more empirical data

to calibrate and verify models. Furthermore, models often neglect transient load scenarios and rely on steady-state assumptions, which limits their applicability to real-world systems such as electric vehicles or hand-held tools.

To this end, Mohamed et al. **[21]** present a notable exception. They used a transient LPTN model to simulate dynamic loading in YASA-type AFPMSMs, providing insights into thermal behaviour under overload and intermittent duty cycles. This study provides critical insight into the thermal headroom and resilience of AFPMSMs like YASA under non-continuous, real-world conditions, showing that motors can be significantly derated in size without compromising performance, as long as thermal constraints are respected. The authors also observed that lower rotational speeds do not always reduce operating temperature—highlighting the importance of accounting for the interaction between heat generation and cooling effectiveness at various speeds.

Complementing this, Grunditz **[4]** provides a comprehensive example by developing a detailed lumped-parameter thermal network model for a V-shaped permanent magnet synchronous machine (PMSM) tailored for battery electric vehicle (BEV) applications. The model includes discrete thermal nodes for stator windings, yoke, teeth, rotor, shaft, and air regions, allowing accurate prediction of transient and steady-state temperature profiles. Special attention is given to the stator winding region, where localized copper losses dominate heat generation.

Lyashenko et al. **[22]** addressed one of the persistent challenges in electric machine thermal modelling: accurately capturing heat transfer in multilayered structures with uncertain interfacial conditions. Lyashenko et al. **[22]** developed a mathematically rigorous model for multilayer cylindrical systems with uncertain boundary conditions, capturing thermal interactions more accurately than traditional models. Their work highlights that simplified LPTMs may fail in systems where internal layering and anisotropic materials dominate heat transfer behaviour—conditions increasingly common in modern electric machines.

Our literature review shows that while considerable progress has been made in thermal modelling of AFPMSMs, studies often prioritize system-level performance analysis over the detailed thermal behaviour of individual components—particularly the stator and windings. There is limited exploration of how thermal gradients evolve within critical substructures like the stator teeth, yoke, or end-windings, especially in asymmetrical, single-sided configurations. This gap is critical because effective thermal management—and by extension, reliability—hinges on precise understanding of where and how heat is generated, accumulated, and dissipated within the stator-winding assembly.

This thesis addresses these critical gaps by developing and experimentally validating a component-level LPTM specifically adapted to the SMC stator and

winding of a single-sided axial flux electric motor (AFEM). Unlike existing system-level approaches, this work focuses on accurately modelling heat generation, distribution, and dissipation within geometries that are not necessarily symmetrical. The result is a novel thermal characterization framework that integrates experimental measurements with analytically derived and empirically calibrated thermal parameters.

3 Theoretical Background

As the previous sections have already introduced the concept of thermal modelling on a basic level, this section will focus on how we tackled the specific task at hand. Many generalities may be postulated about thermal modelling however, when dealing with specific cases, the intricacies grow ever more important. Hence, we have tried to break down our approach to the problem in a simple and structured way, allowing the reader to recreate the work for their own specific scenario if necessary. The model design process went through a several iterations before arriving at a model with a good balance between simplicity, accuracy and adaptability. With this in mind, we will first focus on the fundamental functional principles applied to all model iterations, then we will focus on each individual iteration, and its specific uniqueness. The modelling results and the strengths and weaknesses of each iteration will be addressed in section 3 and 4 respectively.

3.1 Functional Principles

Though each iteration is set up differently, the fundamental basic principles are all the same. It is important here to once again reiterate the fact that we are aiming at a relatively generalised thermal model, meaning we are not interested in the temperature evolution of each individual wire but rather a more global trend of the system and the temperature distribution across the stator. In practice what this means is that a large number of simplifications can be made to facilitate the model construction and solution, while simultaneously maintaining fairly accurate results. All our models are based on the idea of a lumped parameter thermal network (LPTN), which necessitates the Biot-number of a system to be smaller than 0.1 **[13].** The Biot-number is a simple comparison of the thermal conduction resistance of a system with its thermal convection resistance, see **equation 1**. Though not explicitly calculated in this paper, it was checked for each model to ensure the assumptions made were valid.

$$Bi = \frac{R_{conduction}}{R_{convection}} \ll 0.1 \qquad \textbf{(1)}$$

To check the Biot-number a segmentation of the real-world physical system must be undertaken to allow for the nodalisation and subsequent LPTN to be set up. A basic list of all assumptions made for the models is shown below.

Assumptions used in all models:

1. The real-world object can be segmented into several discrete volumes
2. These volumes have a uniform temperature within them
3. Each volume is represented by a node in the thermal network
4. Each node has a given thermal capacitance
5. Each node can heat up via heat generation or heat flow from neighbouring nodes
6. Between two nodes the heat transfer is one dimensional
7. The heat transfer coefficient (k) is constant over time
8. The convective heat transfer coefficient (h) is assumed constant in all directions
9. The convective heat transfer coefficient (h) is assumed constant over time

Given this basic list of assumptions, one may now proceed to the actual segmentation and geometrical simplification of the coil. Due to our need to only calculate general temperature trends, some serious geometric simplifications must be applied to allow the system to remain easy to calculate and visualise. All the components, especially the copper wire, of the coil/bobbin assembly have their shapes morphed into a different form. The final shape the modelled coil will have, is a topic of much debate and many papers propose new shapes and simplification methods to achieve the desired results. The authors of **[23]** for example suggests an approximation using multiple coaxial cylinders to represent the coils copper and insulation layers. In this paper we have decided to keep all shapes rectangular, as this will greatly ease the calculations regarding surface areas and heat transfer. Though the shape itself is no longer geometrically accurate to the coil, the aim is to make geometric simplifications, that are still somewhat tied to real-world dimensions of the coil. By doing this and comparing the modelled results to the experimental ones, a scaling factor may later be added to allow the model to accurately represent the thermal behaviour of the coil. To better understand the geometric alteration the **Figure 1** below may be consulted.

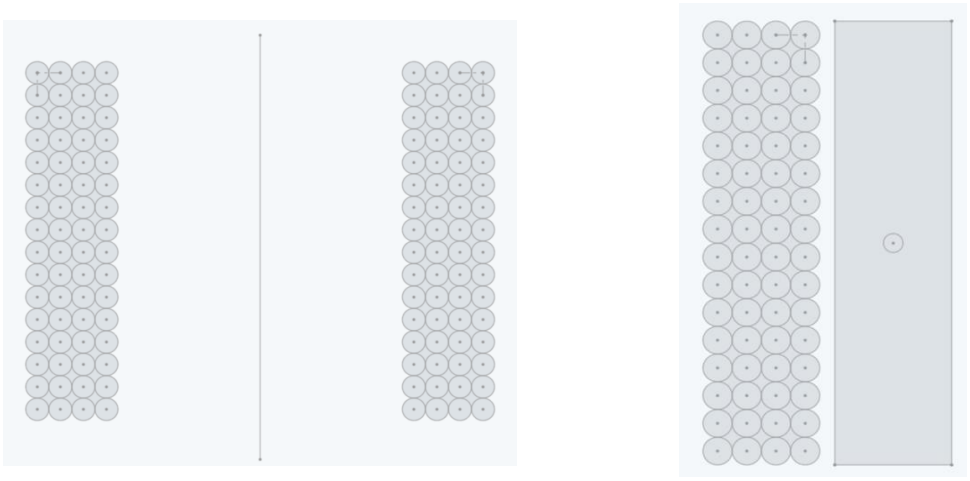

Figure 1: Drawing of geometric simplification

The left side of **Figure 1** shows a coil cut in half with the wires exposed. The right side of the figure shows a rectangle with the same exterior dimensions as the stacked wires in the coil. This rectangle will serve as the geometrically simplified coil. Additionally, since the thermal conduction within the copper itself is very high compared to the conduction to the bobbin or the convection, the coil is "unravelled" and is represented as a single cuboid shape. The length of this rectangle is the length of one single loop of wire around the bobbin. This may be seen in **Figure 2**. The wound coil is on the left in blue and the simplified cuboid is on the right in grey. This representation is aimed at furthering the reader's understanding of the fact that a coil with individual wires may be simplified into a different geometric shape. Though the geometric parameters have changed and will influence things like the value of a thermal resistance, some parameters, such as copper mass, are not changed to keep the thermal capacity of the model the same as the real world.

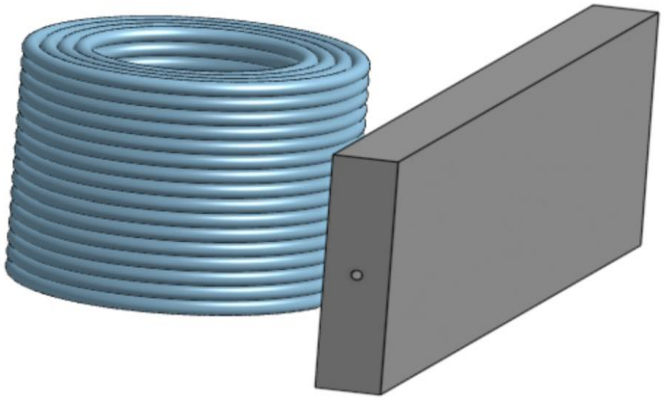

Figure 2: 3-D Geometric simplification of the coil

4 First Iteration Model

4.1 First Iteration Methodology

Having established a good understanding of the basic principle used in the models, one may now proceed to get into the intricacies of the first model. The initial model is purposefully extremely simple in order to act as a proof of concept. Should this model give good results, then further models may be developed, or the existing one may be expanded upon, to allow for a higher resolution in terms of thermal behaviour. The first iteration is essentially the simplest model described in **section 3.1**. It is meant to represent the thermal evolution of only the coil on its bobbin, in free space. The coil and wire insulation are modelled as two cuboid shapes, where the insulation is a thin layer covering the copper cuboid. An illustration of this may be seen below in **Figure 3**.

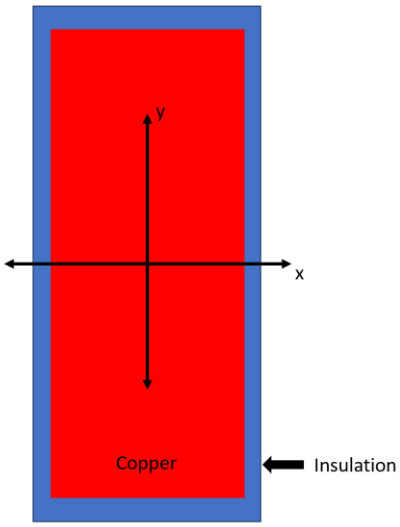

Figure 3: Illustration of 1st iteration simplification

As mentioned in the previous section, the dimensions of the copper cuboid and the thickness of the insulation layer are derived directly from the dimensions of the real-world coil. Given the estimated length of the copper wire through all turns of 5.545 m and the given number of turns (62) the final length of the cuboid is calculated in **equation 2** below.

$$\frac{5.545\ m}{62\ Turns} = 89.443 \cdot 10^{-3}\ m \qquad \textbf{(2)}$$

The height and width are similarly determined based on the coil dimensions. The copper diameter is given as $1.217 \cdot 10^{-3}\ m$, and we know that the coil has 4 layers horizontally and 16 layers vertically. From this the height and width are derived in **equations 3** and **4** below.

$$Width = 4 \cdot 1.217 \cdot 10^{-3}\, m = 4.87 \cdot 10^{-3}\, m \quad \textbf{(3)}$$

$$Height = 16 \cdot 1.217 \cdot 10^{-3}\, m = 19.47 \cdot 10^{-3}\, m \quad \textbf{(4)}$$

The insulation thickness is calculated in a similar fashion for the x and y faces of the cuboid. The insulation thickness per wire is given as $17.375 \cdot 10^{-6}\, m$. From the cuboid centre to the x surface, we have two wires and from the centre to the y surface we have eight wires, therefore the insulation thickness on the x surface is given as: $2 \cdot 17.375 \cdot 10^{-6}\, m = 34.75 \cdot 10^{-6}\, m$, and on the y surface is given as: $8 \cdot 17.375 \cdot 10^{-6}\, m = 139 \cdot 10^{-6}\, m$.

Having covered the geometric dimensions of our model, we can now focus our attention on its thermal properties. In this first basic model, the entire coil is essentially condensed to a single node in our LPTN. The three main factors needed to set up a thermal network are: the thermal capacity, the generated heat, and the thermal resistances. The capacity is simply given by **equation 5** and is considered constant over time.

$$C_{th} = c_p \cdot m_{cu} = 0.385\ \frac{J}{mK} \cdot 45.46\ g = 17.5\ \frac{J}{K} \quad \textbf{(5)}$$

The generated heat (dissipated power) is calculated in **equation 6**. It is ramped up linearly as the coil heats up based on a rate determined from experimental data.

$$P_d = R_{el} \cdot I^2 = 0.0822\ \Omega \cdot (10\ A)^2 = 8.22\ W \quad \textbf{(6)}$$

The determination of the thermal resistances in the circuits is a little trickier, as it is dependent on material thickness and surface area, which varies in x and y. The definition of the resistance values will be broken down into two main sections; conduction and convection thermal resistances, which are shown in **equations 7** and **8** respectively. The conduction resistance is then again separated into copper and insulation.

$$R_{th,\,conduction} = \frac{l}{k \cdot A} \quad \textbf{(7)}$$

$$R_{th,\,convection} = \frac{1}{h \cdot A} \quad \textbf{(8)}$$

Having now determined all the factors needed to build the singular node thermal network, we can represent it in an electrical analogy as is shown in **Figure 4** below.

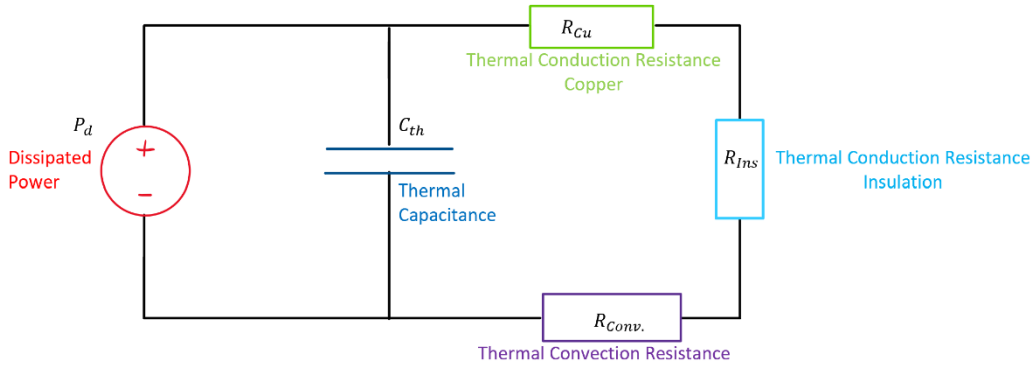

Figure 4: Basic thermal circuit representation

This simple system may then be solved for the temperature evolution using a differential equation, derived from the first law of thermodynamics. The solution to this differential equation can be seen in **equation 9**. $\Delta\theta$ represents the temperature change over time, $\Delta\theta_0$ represents the previous temperature difference to ambient before the heating is begun, τ_{th} is the thermal time constant, R_{th} is the thermal resistance, determined by summing the three resistances from **Figure 4**, as they are connected in series, and P_d is the dissipated power.

$$\Delta\theta = \Delta\theta_0 \cdot e^{-\frac{t}{\tau_{th}}} + R_{th} \cdot P_d \cdot \left(1 - e^{-\frac{t}{\tau_{th}}}\right) \qquad \textbf{(9)}$$

The first part of the equation represents the effects of previous heating and the second part of the equation represents the effects of the current heating. So, in words, the equation might be expressed as heat energy = stored energy + generated energy. The solution to the first iteration model and a comparison to the experimental results are reported in **section 4.3**.

With all this data what we are essentially doing is trying to find an equivalent one-dimensional heat transfer problem whose parameters match the real-world results. We can see in the results section that when taking parameters directly from real world dimensions and applying them to a 1-D problem we get slightly skewed results. Some optimisations and parametric studies are therefore conducted to allow the simulated data to match the measured data.

4.2 First Iteration Experimental Setup

The experiments that were undertaken in this paper were done to validate the results of our model, as well as allow us to apply accurate initial conditions. As the development of the model went through a few iterations, some of which have been left out of this paper for the sake of simplicity, various tests were conducted to validate different scenarios and to ensure the flexibility of our model.

Fundamentally, each experiment consisted of one coil placed onto either a stator resting on an insulating material or simply placed on the insulation material directly. In the case of the first iteration model only a coil was placed on the foam without the stator. A range of currents was then passed through the coils for a specific time period, and the temperature in various locations of the system was recorded with K-type thermocouples. Great importance was placed on ensuring that the system would be as isolated as possible. The object of interest was placed on an insulating material, ensuring that the table or ground would not act as a heat sink, and the whole system was placed inside a large box with high walls, that was open at the top. The box opening allowed for convective heat transfer to occur, while the high walls prevented any circulation currents in the room from altering the convection effects. It was important to isolate the convection term to purely natural convection in the simulations, since the calculation of convection coefficients is an extremely sensitive and complex topic. For a better understanding see **Figure 5** below.

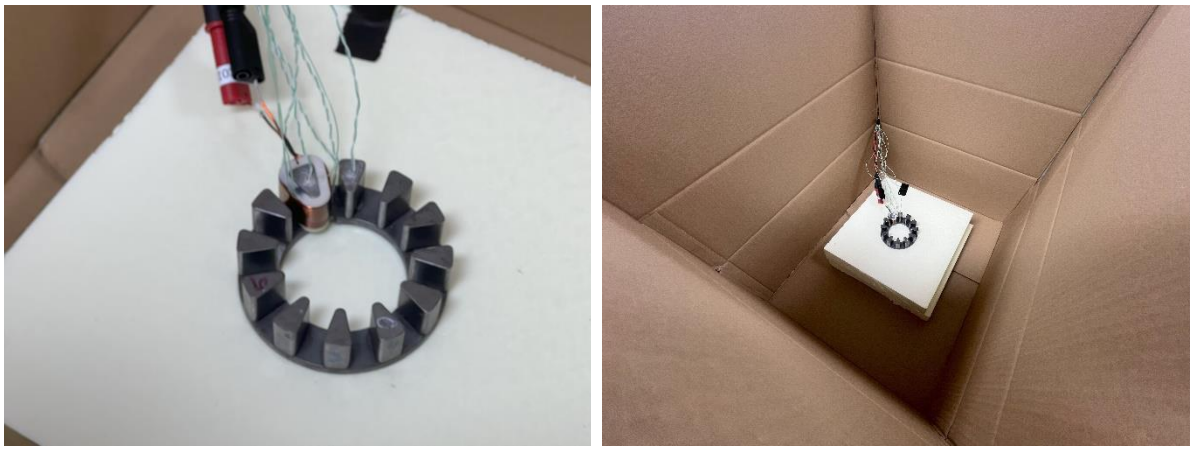

Figure 5: Coil on stator, DC experimental setup

4.3 First Iteration Results

Overall, the results of the first iteration model seem quite promising. **Figure 6** represents the initial estimation in x and y directions and compares them to the measured experimental data.

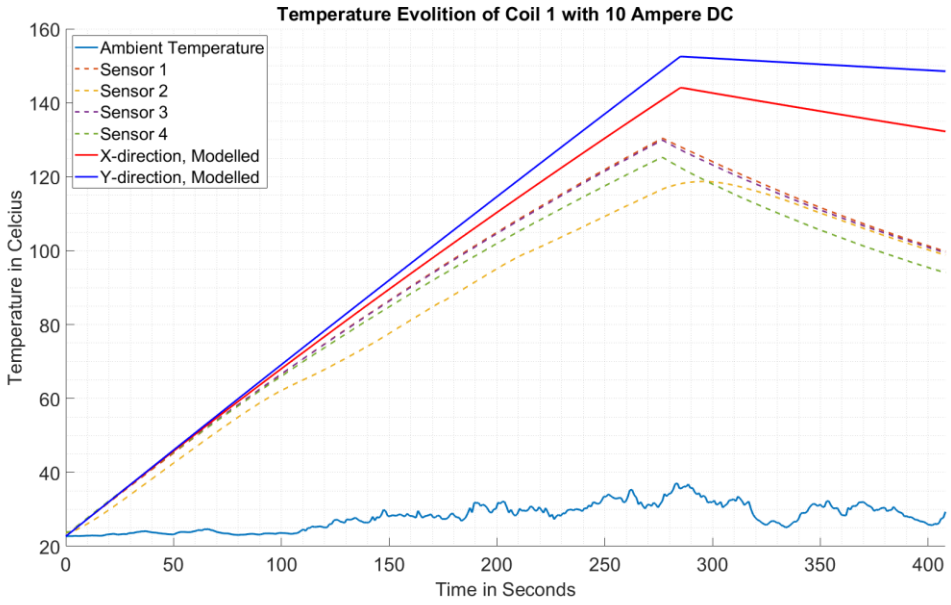

Figure 6: First iteration temperature evolution

When looking at the graph a few oddities may be observed. The ambient temperature seems to spike randomly, however this is due to a poor placement of the sensor. It was placed somewhat above the coil and hence was influenced by the convective heating from the coil. Additionally, one of the four sensors (Sensor 2) in the coil has a very strange and unexpected temperature evolution compared to the others. As the sensors are placed in between the wire layers, during the winding process, it is possible that the sensor got damaged or lodged in the bobbin material, which might explain the odd results. Considering we are only interested in the general global trend of the system an average temperature was then taken between the three sensors with accurate readings.

As can be seen quite clearly the x-direction model is much closer to the reality of the measured results and is therefore taken as the starting point of our parametric tuning to align modelled with measured results. This way we attain a better starting point for converting the coil into a one-dimensional equivalent problem. After conducting some parametric studies on the effects of the convective heat transfer coefficient (h) and a scaling factor for the area of the cuboid surface area, the results look far more promising. It was found that with a h value of 20 for natural convection

and an area scaling factor (A.S.F.) of 1.8 the best results were achieved, they are illustrated in **Figure 7**.

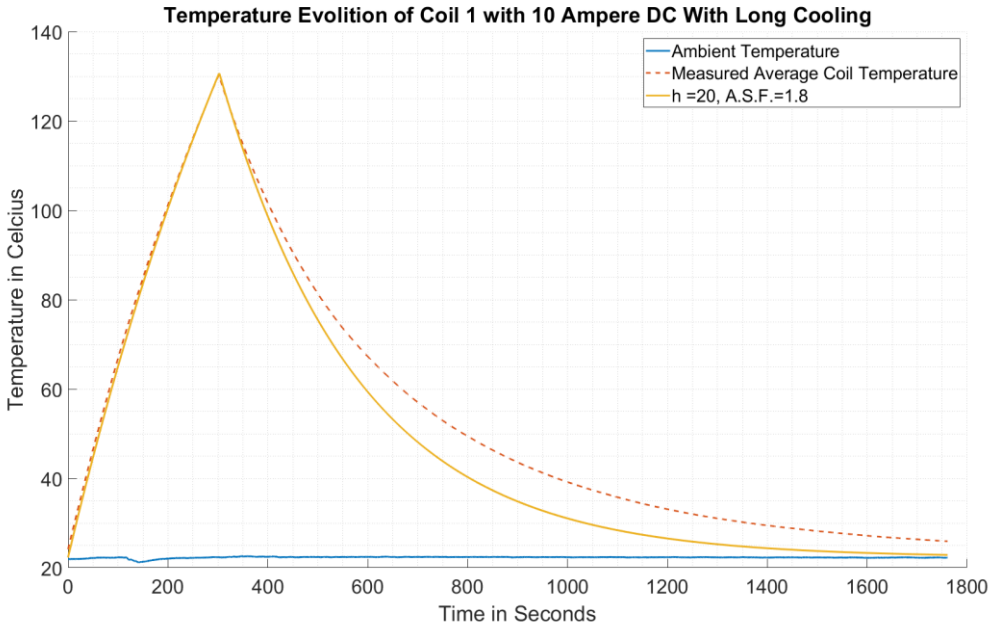

Figure 7: First iteration temperature evolution with curve fitting

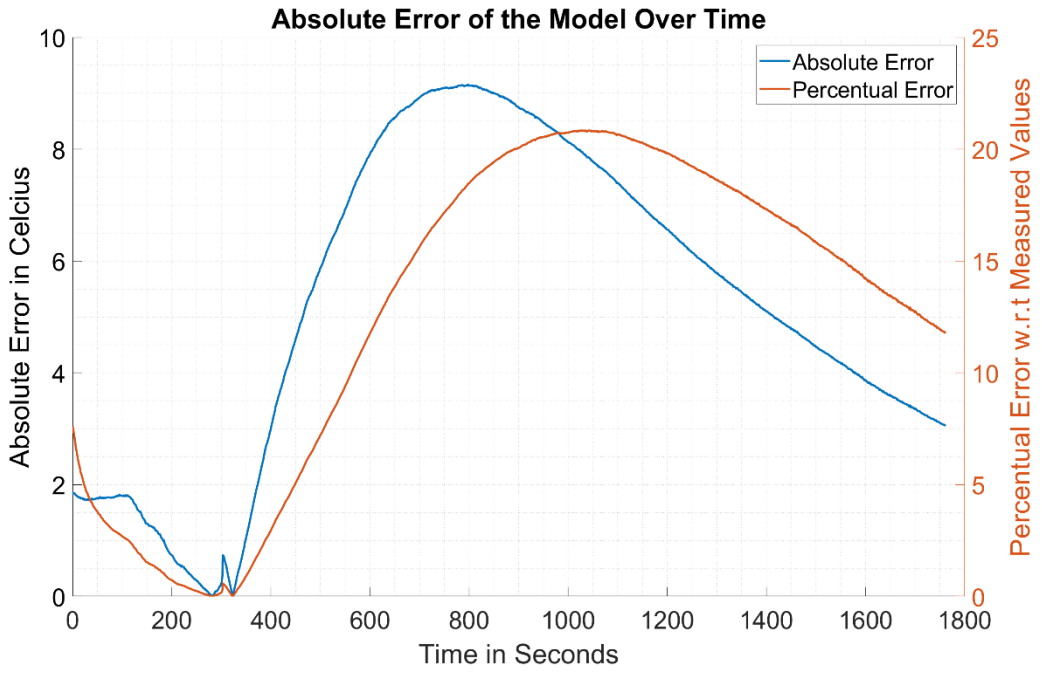

Figure 8: First iteration error

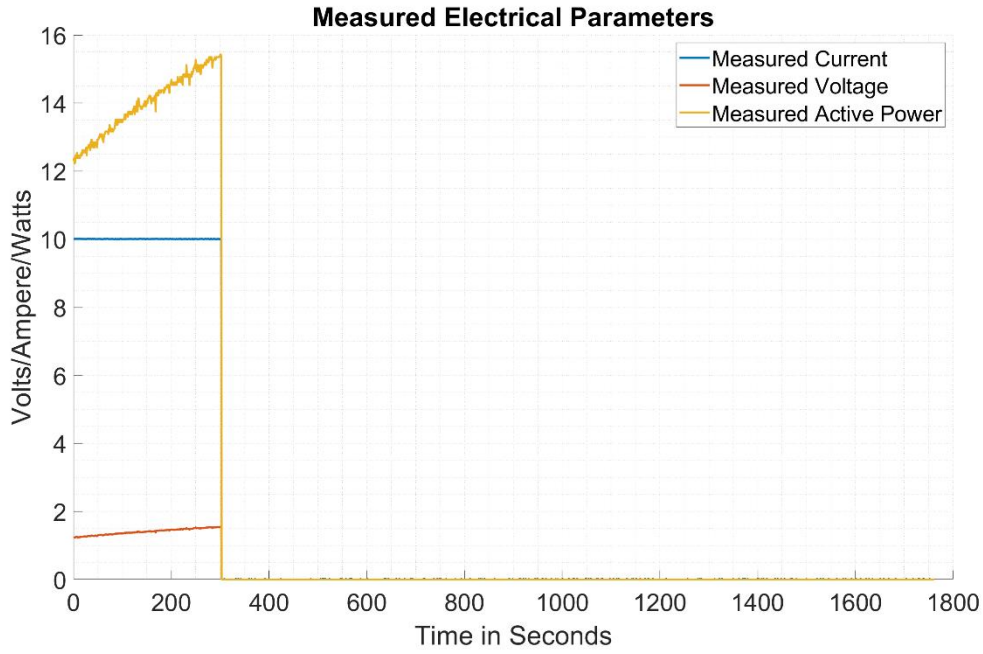

Figure 9: Measured electrical data

It may be noted in **Figure 8** that the maximum absolute error of this model is less than $10°C$, which is within our targeted level of model accuracy for the first iteration. Another Important factor to be considered is the heating time. During the experiments it was decided not to exceed a temperature of $130°C$ to avoid damaging the coil. Subsequently, the length of the heating phase was adapted to this restraint.

4.4 First Iteration Discussion

This first iteration was designed with a clear objective: to test whether a simplified, lumped thermal model could reasonably approximate the temperature evolution of the coil under DC loading. The underlying hypothesis was that even with geometric simplifications, a model based on basic heat transfer principles could still produce useful results.

To explore this, the coil was represented as a uniform copper cuboid. This abstraction allowed for the construction of a single-node thermal network, where the coil's thermal behaviour was solved analytically using resistance-capacitance analogies. As a result, the model required minimal computational resources and was easy to implement—ideal for quickly capturing broad thermal trends.

However, this simplicity introduced several physical omissions. The model did not account for the real-world complexity of the coil structure, including insulation, air

pockets (within the winding), and thermal contact resistance with the bobbin. These omissions reduced the effective surface area available for convective cooling and overestimated conductive heat transfer. Consequently, the model initially predicted higher-than-observed coil temperatures, especially during the cooling phase.

To improve accuracy, two key parameters were adjusted: a surface area scaling factor and the natural convection coefficient. These changes helped correct for the simplified geometry and resulted in significantly better alignment with experimental data—reducing the maximum error to within 10 °C and heating-phase error to within 5 °C. The assumption of constant material properties and fixed heat transfer coefficients further streamlined the model and enabled smooth, predictable temperature curves during heating. This confirmed that copper's high conductivity supports the assumption of uniform internal temperature within the coil during continuous DC heating.

Despite these strengths, the model struggled to reproduce cooling behaviour accurately. This limitation was directly caused by the use of a fixed convection coefficient, which does not capture the temperature-dependent nature of real-world convection. Additionally, while the model did not reach a true steady state, it is likely that a different convection coefficient would apply at higher temperatures than those observed during the earlier, lower-temperature transients used for parametric tuning. In reality, as the coil cools and its surface temperature drops, natural convection becomes less effective. By keeping the convection coefficient constant, the model overestimated cooling rates. This suggests that future versions should allow heat loss to vary with temperature to better capture cooling dynamics.

Validation data came from four thermocouples embedded in the coil. One sensor exhibited abnormal readings, but averaging the remaining three provided a reliable benchmark. However, additional sources of error should be acknowledged. These include potential inaccuracies in sensor calibration, local thermal gradients at the point of contact, and the influence of sensor placement, which may not precisely capture the core temperature due to positioning within the winding structure. Contact resistance between the thermocouple and the copper could also introduce measurement lag or offset. Despite these limitations, the strong match during the heating phase confirmed that, under steady DC current, the lumped-node assumption is valid when internal temperature gradients are small.

The main achievement of this first iteration lies in its successful demonstration that simplified geometry, and thermal networks can still produce meaningful predictions. This supports the broader contribution of the study: providing a lightweight methodology that can serve as a foundation for more advanced thermal models. In doing so, it shows that simplified thermal models are not only computationally efficient but also potentially suitable for early-stage design analysis and real-time applications.

Overall, this first iteration proved that a basic lumped parameter model can effectively capture key thermal behaviour of the stator coil under DC loading. It balanced simplicity with sufficient accuracy and laid the groundwork for further development. While not fully predictive without calibration, its success highlights the value of selective simplification in thermal analysis. The model is particularly effective for estimating heating trends quickly and is well-suited for fast, low-cost predictions in simple component testing. However, its assumption of constant cooling conditions limits accuracy during the cooling phase—an important consideration for more detailed design studies.

5 Second Iteration Model

5.1 Second Iteration Methodology

Though the first iteration model did result in fairly accurate modelling of a single coil, especially during heating, it has very limited applications for the real world. Its main use case would be for a very quick and fast thermal modelling of basic components in isolation from a larger system. To combat these limitations, it was decided to focus on a more complex and adaptable thermal model for a system with more intricacies, such as a coil on a stator.

In pursuit of this goal, the general approach strategy was necessarily altered to accommodate the new requirements. The first iteration relied on an analytical solution to the differential heat equation to determine the thermal behaviour of each node in the lumped parameter network, in that case a single node. This has its benefits in terms of result accuracy but brings an increasing complexity with it, as the nodal network expands and grows. The only other solution to the problem is then quite obviously to attempt to solve the differential equation numerically. In our case we decided to use the Euler forward differencing method, since all the initial conditions are known and it lends itself quite nicely to being implemented into a number of programming languages. For all our solution methods we used MATLAB because of its great flexibility in using and setting up matrices, a link to all the code in this paper is shown in **[29].**

While the Euler forward method is a natural first choice due to its simplicity and ease of implementation, especially when small time steps are acceptable, it is worth noting that more advanced numerical methods can offer improved stability and efficiency under certain conditions. Predictor-corrector schemes such as Heun's method or higher-order Runge-Kutta methods (e.g., RK4) provide greater accuracy and numerical stability for stiff or rapidly changing systems, often allowing for larger time steps without compromising solution quality. Implicit methods,

although computationally more involved per step, can also be advantageous in stiff systems where explicit solvers require prohibitively small time steps for stability. In practice, while these methods involve a higher per-step computational cost, they can yield overall time savings in large or complex simulations by reducing the total number of required steps. Therefore, for future expansions of the model, especially those involving strong nonlinearities or tight thermal coupling, consideration of such alternative solvers may prove beneficial.

In essence, as all thermal modelling does in some form or another, the starting point for this model is finding a solution to the Fourier heat equation shown in **equation 10**.

$$\frac{\delta}{\delta x}\left(k \cdot \frac{\delta T}{\delta x}\right) + \frac{\delta}{\delta y}\left(k \cdot \frac{\delta T}{\delta y}\right) + \frac{\delta}{\delta z}\left(k \cdot \frac{\delta T}{\delta z}\right) + q_v = \rho\, c_p\, \frac{\delta T}{\delta t} \qquad \textbf{(10)}$$

Where k is the materials heat transfer coefficient, q_v is the rate of heat generation, ρ is the density and c_p is the specific thermal heat capacity. This equation is somewhat complex to deal with and must therefore be simplified to allow for a quick and easy solving algorithm. The way to simplify this equation is to make a few important assumptions. In the forward Euler differencing method, we are essentially breaking down our equation into lots of small time-steps and making a linear approximation of the analytical solution per each step. The smaller the step, the more accurate the result of this numerical solution will be at the cost of longer computational times. Furthermore, the lumped parameter approach makes the assumption that heat transfer between two nodes is only one dimensional. With these assumptions in mind, it can be shown that the Fourier equation may be simplified to what is displayed in **equation 11**.

$$\frac{d\,T_i}{d\,t} = \Sigma_j\, \frac{G_{i\,j}\left(T_j - T_i\right) + q_{gen}}{C_i} \qquad \textbf{(11)}$$

Where T_i is the temperature of a node of interest i, T_j is the temperature of a neighboring node j, $G_{i\,j}$is the thermal conductance between the two nodes i and j, q_{gen} is the generated heat in the node i, and C_i is the thermal capacitance of the node i. The ways to calculate C_i and $G_{i\,j}$are shown in **equations 5** and **7/8** respectively. G is simply the inverse of R. To then solve this system the steps as shown below in **equations 12 - 15** should be followed.

$$T_i\,(t_{new}) = T_i\,(t_{old}) + \frac{1}{C_i}\int_{t_{old}}^{t_{new}} (\Sigma_j\; G_{i\,j}\left(T_j - T_i\right) + q_{gen})\, dt \qquad \textbf{(12)}$$

$$\dot{Q}_i \;=\; (\,\Sigma_j\, G_{i\,j}\left(T_j - T_i\right) + q_{gen})\Big|_{t_{old}}^{t_{new}} = const. \qquad \textbf{(13)}$$

$$\frac{1}{C_i}\int_{t_{old}}^{t_{new}} (\Sigma_j\; G_{i\,j}\left(T_j - T_i\right)\; + q_{gen})dt = \frac{\dot{Q}_i\,(t_{new} - t_{old})}{C_i} = \frac{\dot{Q}_i}{C_i}\,\Delta t \qquad \textbf{(14)}$$

$$T_i(t + \Delta t)\; = T_i(t) + \frac{\dot{Q}_i}{C_i}\,\Delta t \qquad \textbf{(15)}$$

This solution pivots heavily on the assumption made in **equation 13**, that the heat flow is constant in time. Although in reality this is not the case, if a small enough time step Δt is chosen, then it can be used as a valid method for approximating thermal behaviour over time. In fact, the choice of the time step is crucial for the algorithm to work properly. A too large time step will lead to instability in the system and create peculiar results. A good rule of thumb for determining an adequate time step size is shown in **equation 16**.

$$\Delta t_{min} = 0.9 \cdot \frac{C_{min}}{G_{max}} \quad \textbf{(16)}$$

Where C_{min} is the smallest thermal capacity in the nodal network and G_{max} is the largest thermal conductance in the thermal network. This is fundamentally the mathematical basis of everything that is about to be expanded upon. There are certainly intricacies to be considered but it is vital for the reader to comprehend the previous fundamental mathematical derivation, to ensure a good foundation for understanding some subsequent choices. The mathematical steps shown here are a summary and leave out some aspects that may be of interest for other applications. If a deeper understanding is desired, we recommend reading the papers referred to in **[24]** and **[25].**

On a fundamental level, what this algorithm calculates is to iteratively determine the heat flowing in and out of each node in the LPTN per time step. Previously this took large amounts of computing power, but with modern processors and programs like MATLAB, matrix manipulations have become very easy and fast.

The mathematical solution to the LPTN has been dealt with and the actual nodalisation of our system may now be tackled. As is also reiterated in the literature the actual nodalisation of the physical system is often far more important to the accuracy of results than the usage of different solving algorithms. Due to the time limitations of this thesis, a simplified system was modelled and evaluated. The system chosen was a single coil on a stator tooth, where the temperature evolution

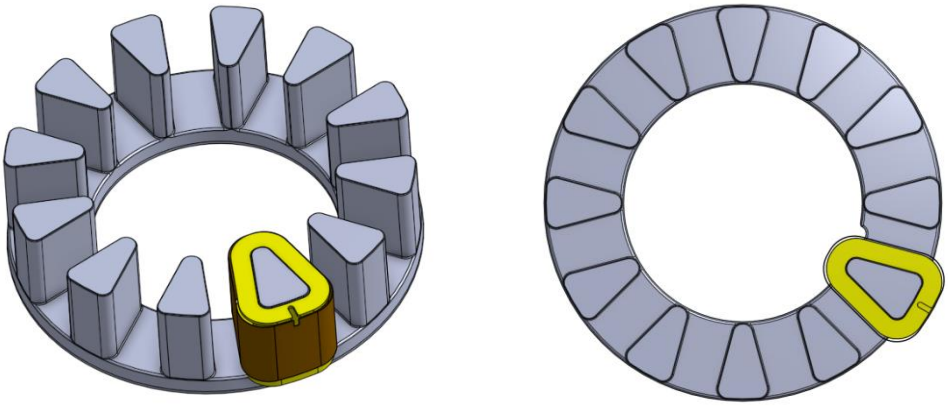

Figure 10: 3-D Render of coil on stator

of the coil as well as the heat diffusion along the stator were monitored. A 3-D rendering of the considered coil on stator system may be seen in **Figure 10**.

From the data of this model, due to the symmetry of the stator, a model of the entire stator may be extrapolated. The approach chosen for nodalisation was to start very simply, with large volumes, and add complexity as needed based on the result accuracy. This allows the solution to be as complex as necessary and as simple as possible. A visualisation of the segmentation, the analogous electrical circuit as well as an approximate overlay of that circuit on the real-world geometry are shown in **Figure 11**, **12** and **13** respectively.

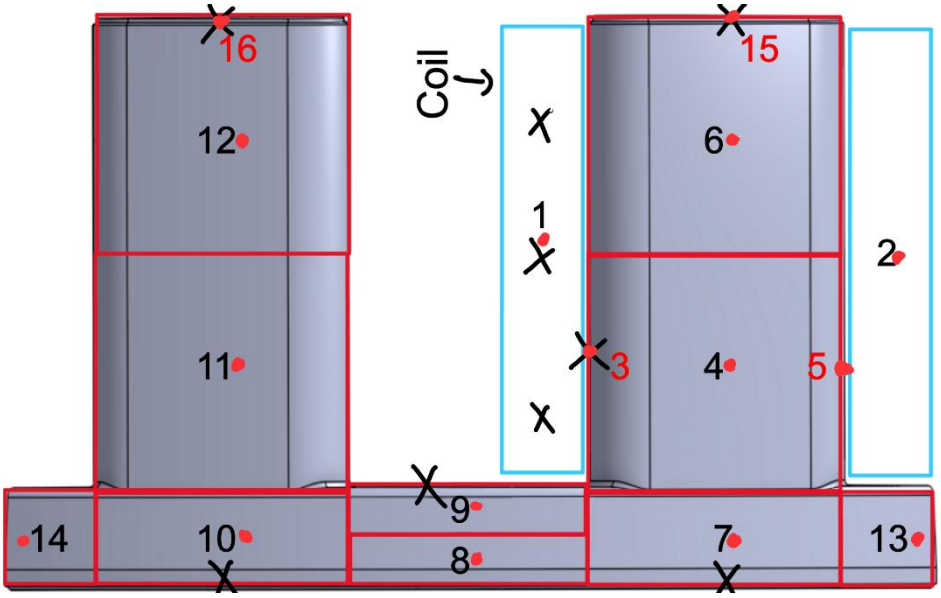

Figure 11: Geometric segmentation of system

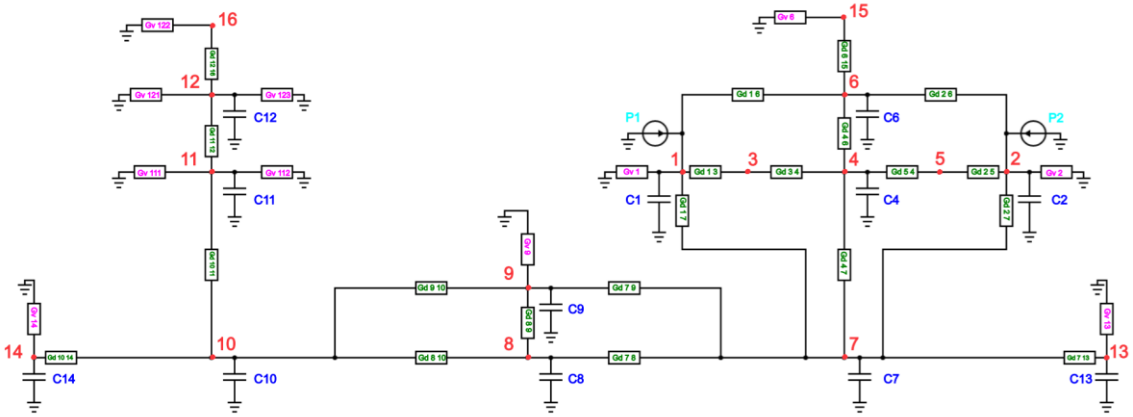

Figure 12: Analogous electrical circuit of coil on stator

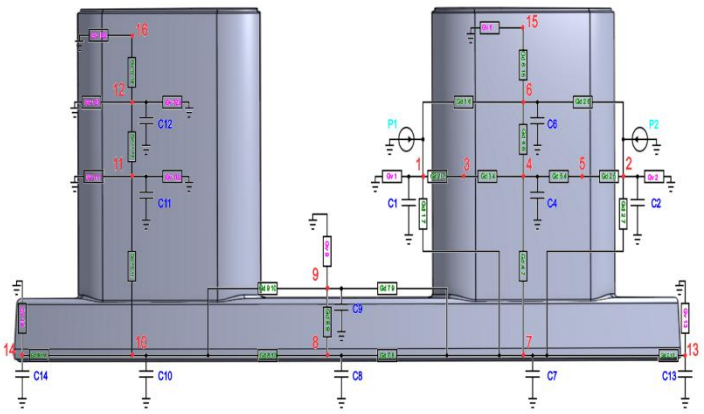

Figure 13: Overlay of the electrical circuit on the stator teeth

In **Figure 11** we can see what volume each node represents. The black crosses represent the sensor location in the real world. A big factor in the choice of segments is where the temperature can be measured in experiments. Though knowing the temperature of the core of the stator may be useful for calculations it is not possible to experimentally confirm the data. This is why nodes 3, 5, 15 and 16 exist; They are considered nodes with zero volume to simulate the actual temperature at the sensor locations. In the code, however, they are given a very small thermal capacitance rather than zero, to avoid errors in calculation. The corresponding surface areas and distances between nodes are taken directly from the CAD model of the stator and compiled in a spreadsheet. These values are then used in combination with the heat transfer coefficients to determine all the conductive and convective thermal conductances in the circuit.

In order to ensure that the solving algorithm and nodalisation method were the only two variables that could be responsible for poor results it was decided to determine the heat transfer coefficients experimentally rather than making a myriad of assumptions. In particular the convective heat transfer coefficient h is extremely difficult to ascertain as it is the result of complex and hard to measure quantities such as fluid motion, viscosities, etc. In fact, entire dissertations have been dedicated to the sole determination of the h value in different scenarios. Additionally for our specific case and due to various design reasons on the electromagnetic side, the stator material is not a solid piece of metal or laminations of electrical steel as is common for electric motors. This stator uses a Soft Magnetic Composite (SMC), which is essentially a metal powder, where each grain is coated in an insulation material. The powder is then pressed into shape with enormous pressures and heat treated. This process leads to many advantageous qualities, in terms of minimising the flow of eddy currents in the stator material, but it brings with it greater complexity in terms of material properties. As one might imagine, the fact that each grain of powder is coated in insulation material leads to poorer thermal conductivity with respect to a pure metal. Furthermore, the enormous pressures used in

production lead to a deformation of the grains which leads to the material having anisotropic characteristics **[26].** The k value of the bobbin material and the copper in the coil were taken from the manufacturer data sheet and **[27]** respectively.

The experimental setups to determine k and h and the resulting data are described in **sections 5.2** and **5.3.1** respectively. To give the reader an idea of the effects this type of material has on the thermal conductivity, here is a brief summary of the results. Pure iron has a thermal conductivity of around 80 $\frac{W}{m\,K}$ **[28].** The experiments showed however that the 5P SMC material used in the stator had a thermal conductivity of around 11 $\frac{W}{m\,K}$ in the pressing direction and around 15 $\frac{W}{m\,K}$ in the direction perpendicular to the pressing.

Having now determined all the parameters of the circuit, the only problem left is to solve the system for a given power input in the relevant nodes. Since the dissipated power from the coil increases with increasing temperature, the power increase during testing runs was recorded and used to determine an approximately linear power increase over the time period in question. For initial tests, a DC current was applied to the coil meaning the only nodes with power generation would be 1 and 2, so the ones representing the coil. When AC currents are used, iron losses will cause there to be power generation inside the stator nodes as well, dependent on their distance from the coil, their size and resilience to eddy current flow.

The calculation of the AC losses was done with many assumptions in mind. As there was no analytical model readily available for the stator under examination, it was deemed outside the scope of this thesis to develop another analytical model for the electromagnetic losses. The approach strategy that was chosen was to use the empirical Steinmetz equation to determine the iron losses in the stator, which can be seen in **equation 17**.

$$P_{Fe} = K_h \hat{B}^{\alpha} f^1 + K_e \hat{B}^2 f^2 \qquad \textbf{(17)}$$

Where $\hat{B}$ is the peak magnetic flux density, f is the AC frequency, and K_h, K_e and α are experimentally determined coefficients. The values of these were ascertained from a database of previous electromagnetic tests conducted by Alvier Mechatronics and Höganäs AB and are displayed in **Table 1**. The calculation of these parameters was repeated in multiple ways and experimentally verified multiple times. The overall results from all test runs did not differ greatly before the 4th decimal, and therefore they may be seen as accurate.

Coefficient	Experimentally Determined Value
K_h	1.10e-01
K_e	4.43e-05
α	1.75

Table 1: Experimentally determined values for the Steinmetz equation

In **equation 17** the iron losses are split into two parts, the first being iron losses stemming from hysteresis and the second stemming from eddy currents. An additional loss that would arise from the usage of AC would be AC losses in the coil. However, since we are considering only a single coil on the stator, the slot will not be filled completely and there will be no induction effects from neighbouring coils. This means that the AC effect inside the coil will be negligible in our current setup. With a complete motor setup, they are of course not negligible, but their calculation may simply be added to the nodes that generate power in the analogous electrical circuit if more accurate results are required.

Regardless of if an AC or DC current is used, the segmentation and solving algorithm will stay the same, the only difference will be an increased number of current generators in the electrical analogy circuit at various stator nodes.

5.2 Second Iteration Experimental Setup

The regular temperature tests of the system were conducted in the same way as described in the first iteration. However, the tests to determine the heat transfer coefficients, both convective and conductive, were set up differently. To determine the convective heat transfer coefficient, it was necessary to measure the cooling rate of the coil. Considering that it usually rests on the stator tooth, a piece of insulating foam was wedged into the middle of the coil, ensuring that the only location for convective heat transfer would be the outside surface of the coil, see **Figure 14**.

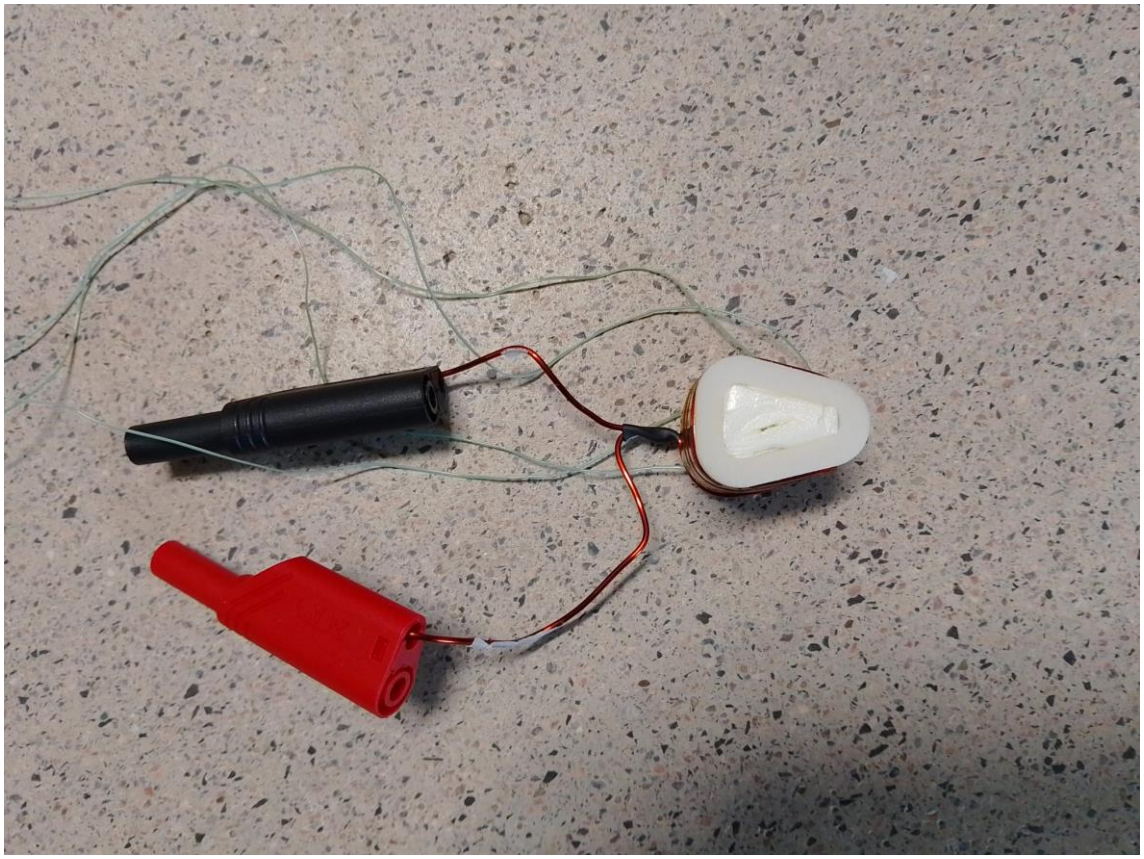

Figure 14: Determining the h value experimental setup

To determine the conductive heat transfer coefficient, a component made from the same material as the stator but with a simpler geometry was chosen for analysis to ease the calculations. In our case a 22x22x22 mm cube of the 5P SMC was analysed. This block was fitted with two thermocouples on opposing sides which were lathered in thermal paste to allow for good thermal conduction between the sensor and the cube, to ensure data accuracy. The cube was then placed inside a large piece of insulating foam with two resistive heaters on one side. Heating one side of the cube and insulating all other sides allows us to approximate pure 1-D heat transfer through the object and eliminate any convective cooling effects. See **Figure 15** for a better understanding of the physical setup. The two halves shown in the figure were closed on top of each other and pressed together using tape, to ensure good contact between the components and good sealing of the gap in the foam. If we assume no cooling is taking place and monitor the temperature evolution on the opposing sides, the algorithm used in the second iteration model can be rearranged to determine the value of k. Of course, no system is perfect, and some small amount of cooling took place during the experiment as well, but to a degree which would be insignificant with respect to the conductive heat transfer heat flow.

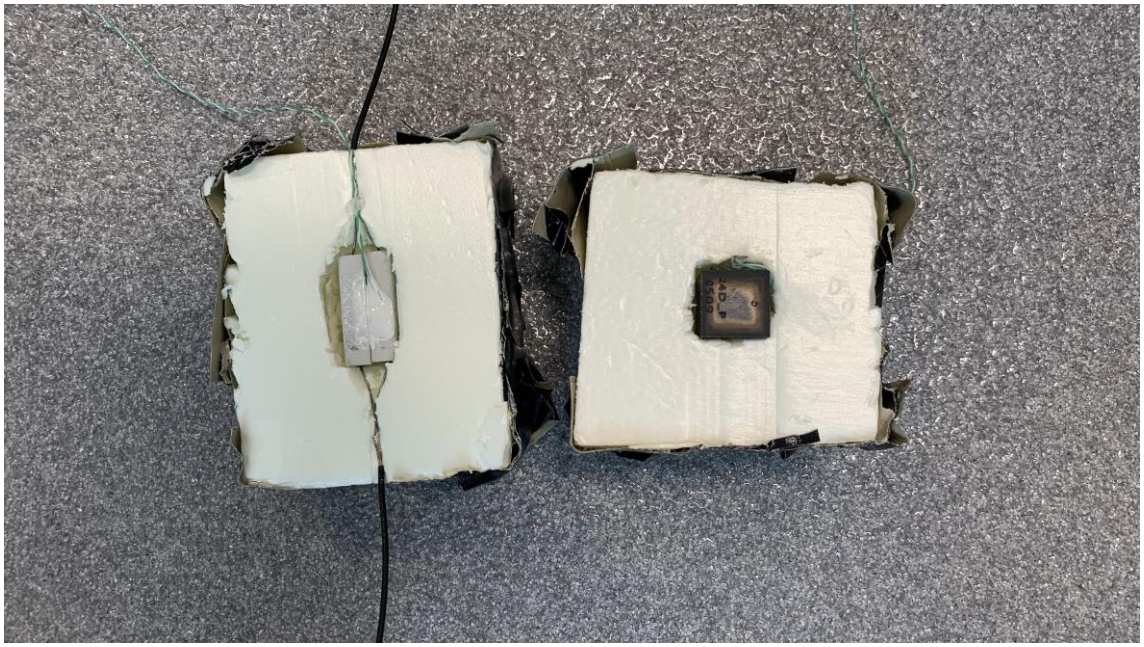

Figure 15: Determining k values experimental setup

Lastly a few modifications needed to be made to run accurate AC tests. As the system in question is very simple, many of the sources of AC losses were not present. Nevertheless, it was attempted to obtain as accurate a result as possible. With this in mind the decision was made to clamp a plate of the same 5P SMC material as the stator on top of the teeth. This was done to close the magnetic circuit of the coil, to allow at least some iron losses to be recorded. However, the maximum frequency that could be obtained by us for such a small load was 100Hz with an RMS current of 13A. This of course will not lead to very high losses but may give indications about the feasibility of the iron loss calculation method. To better understand the setup **Figures 16** and **17** may be observed.

Figure 16: AC experimental setup side view

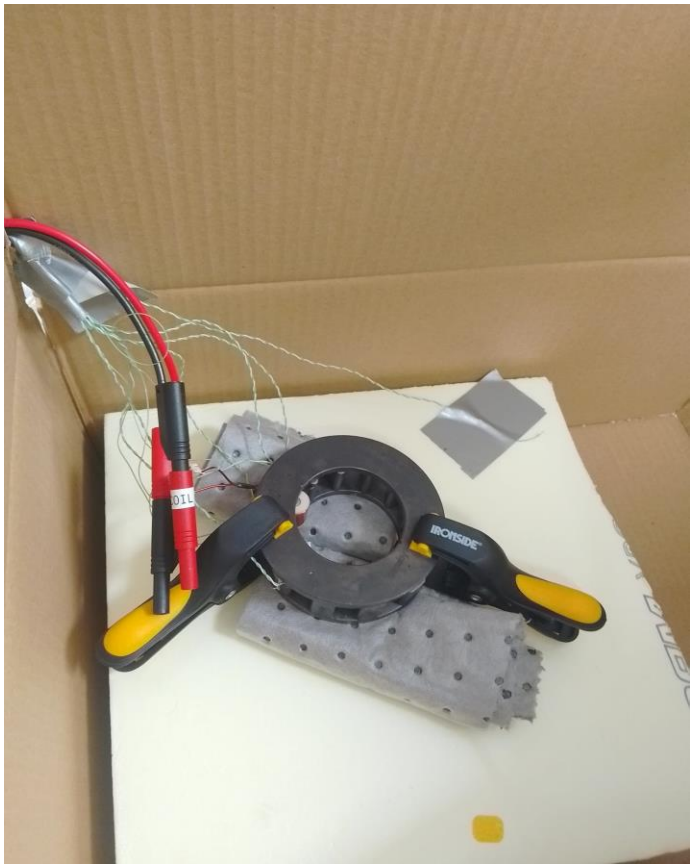

Figure 17: AC experimental setup top view

5.3 Second Iteration Results

5.3.1 Determining Heat Transfer Coefficients Results

The experiments for both of the heat transfer coefficients (h and k) were repeated 3 times each and all yielded very similar results. In **Figure 18** the recorded temperature data is shown and in **Figure 19** the experimental data for the conductive heat transfer coefficient are shown. They were calculated by rearranging the forward Euler differencing equation and determining the value per each time step. Due to sensor inaccuracies, especially when dealing with small temperature increases which is the case per time step, there is a considerable amount of noise in the data. A smoothed curve is overlaid and shows that after an initial transient, the k values for both directions stay relatively constant. The smoothing was conducted using a moving average smoothing, using the movmean function in MATLAB. The final values that were determined were taken as an average of the steady-state section of the graph and were 11.29 $\frac{W}{mK}$ and 15.88 $\frac{W}{mK}$ for the press and perpendicular directions respectively. This calculation assumed a perfect one-dimensional heat transfer which is of course never the case in the real world. The result of this may be a slightly offset final result for the k value. Nevertheless, during the heating phase, the conduction terms is dominant with respect to the convection term and therefore the one-dimensional assumption made is useful for our application.

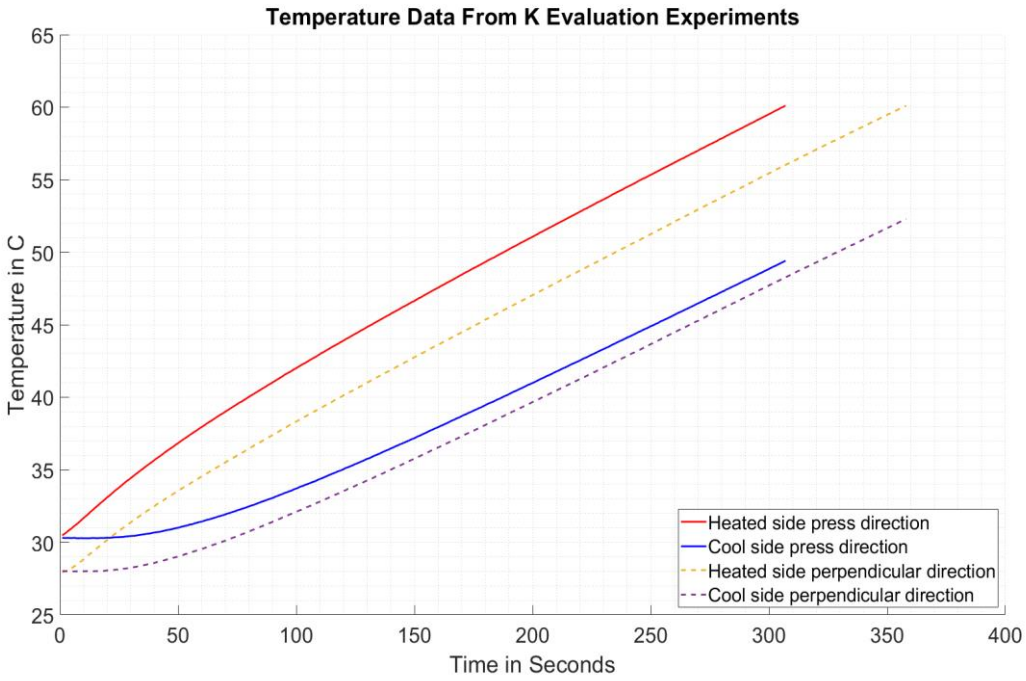

Figure 18: Experimental data for evaluation of k

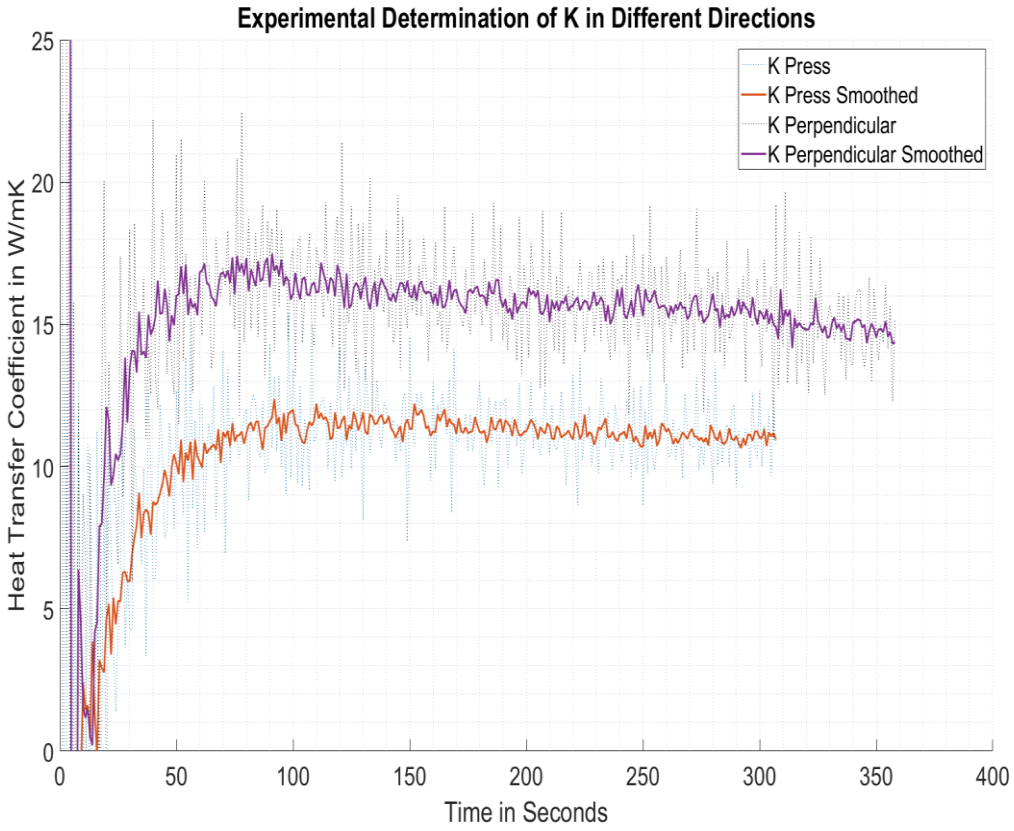

Figure 19: Experimental k value results

The convective heat transfer coefficient h was determined in two ways. Firstly, the cooling curve of the experimental data was approximated with a curve fitting that utilises a single h value for the duration of cooling (**Figure 20**). Secondly, similarly to before, the h value was determined per time step and a smoothed average was overlayed (**Figure 21**). The same moving mean average as for the k value was utilised for the h value smoothing as well. The calculation for both methods were quite different as the first solves the heat equation analytically and determines the h value from the fitted curve's time constant and the second determines the h value from rearranging the forward Euler differentiation per time step. Realistically the second method should yield more accurate results in simulation, since the convective heat transfer varies with varying temperature differences between the fluid and the solid. In fact, in **Figure 21** one may observe a steady decrease in the coefficient's value. As the decrease becomes quite level after an initial transient phase, it was decided to take the mean value of this section as a constant for the duration of the simulations to come. Both methods yielded similar results, with method one having a h value of $19.08\frac{W}{m^2K}$ and method two having an average value of $16.33\frac{W}{m^2K}$, which is in line with common values for natural convection being in the range of $5-25\frac{W}{m^2K}$ **[13].**

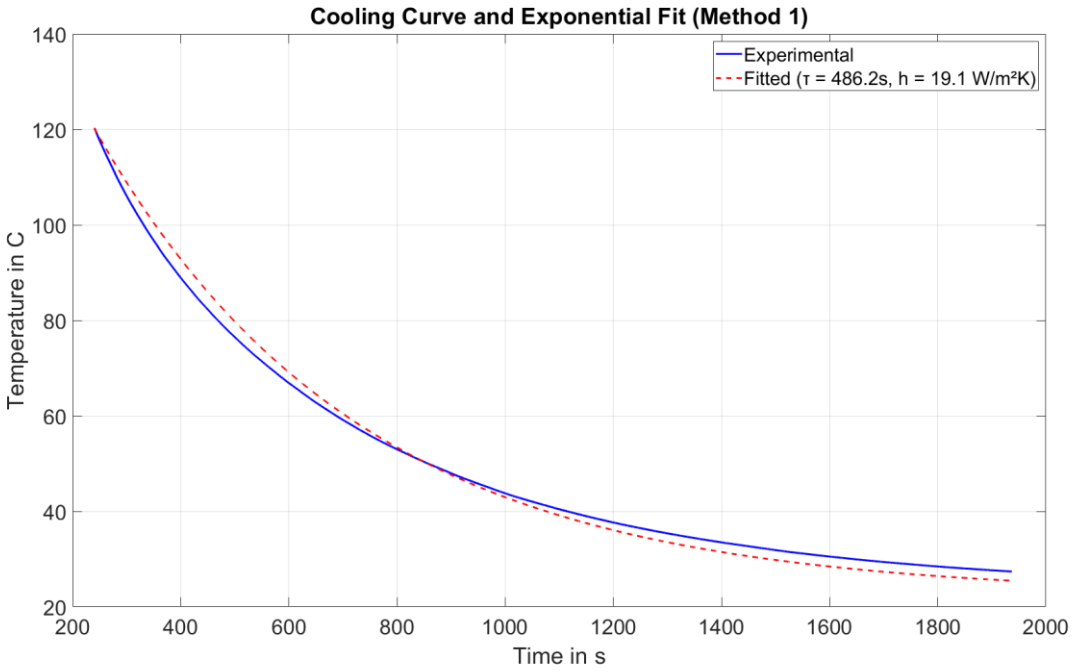

Figure 20: Experimental h value method 1

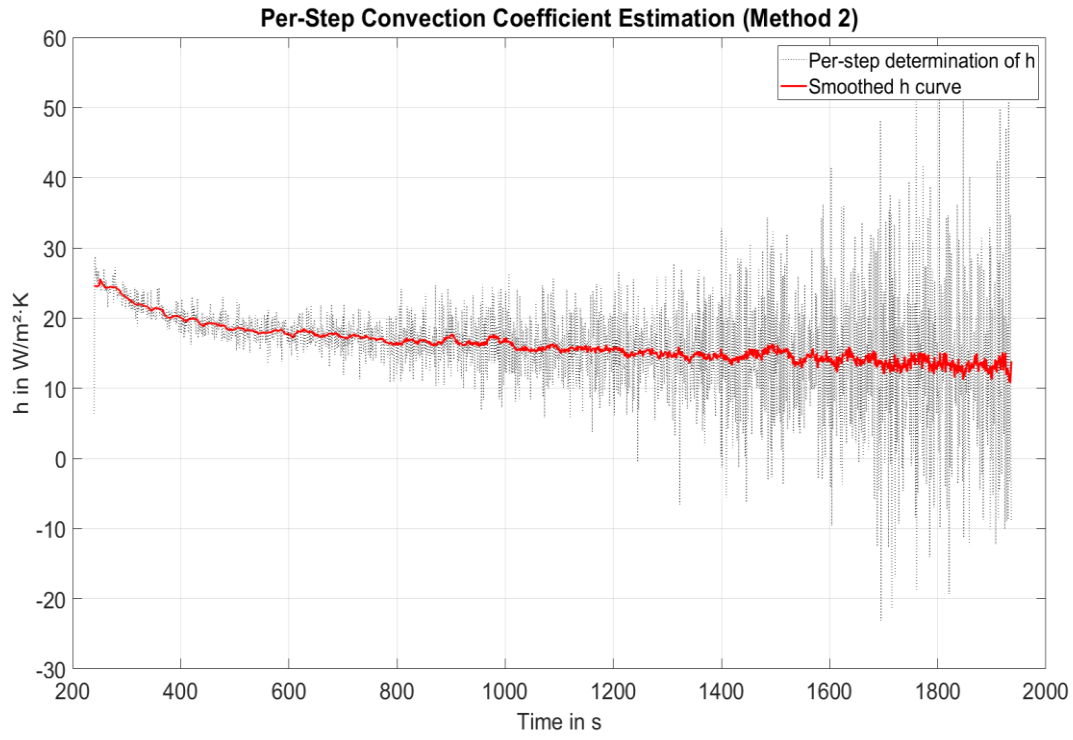

Figure 21: Experimental h value method 2

5.3.2 Total Nodal Network Results

The simulations for the established nodal network of the single coil on the stator were repeated multiple times for different currents. The first run of experiments was done over a relatively short time frame; hence they were repeated in a second run to also ascertain the behaviour of longer cooling. **Figures 22-25** depict the comparison of simulated and measured results and the errors for the first run, and **Figures 26-29** depict the same for the second run. The graphs labelled "*ABC mean*" represent a mean value of all the three sensors placed inside the coil winding, which were labelled A, B and C. The errors chosen were the error for the coil temperature and the error of sensor 2, located between the bobbin and the stator. This error metric was chosen as the coil temperature will always be the hottest and therefore most limiting in terms of performance in the system, and sensor Two was one of the sensors with the highest discrepancy between measured and simulated results. For run 1 we can see that with an increased current, both the absolute error and the percentual error increase slightly. For simplicities sake, test results with further differing currents were not included in this paper but the general trend shown was that with an increase in current the error slightly increased as well. Nevertheless, the overall absolute error in all runs stayed below $10°C$, which is a fairly remarkable result for such a rough nodalisation strategy. Additionally, the absolute error of the coil temperature stayed below $5°C$ in all our test runs. The second run of experiments showed a slightly improved model accuracy on the initial phases, which then gives way to a misaligned steady state cooling temperature. The possible reasons for this will be touched upon in the discussion section below. Overall, the model was able to quite accurately predict the node temperatures, giving an excellent reading for the coil temperature and exceeding some stator node temperatures.

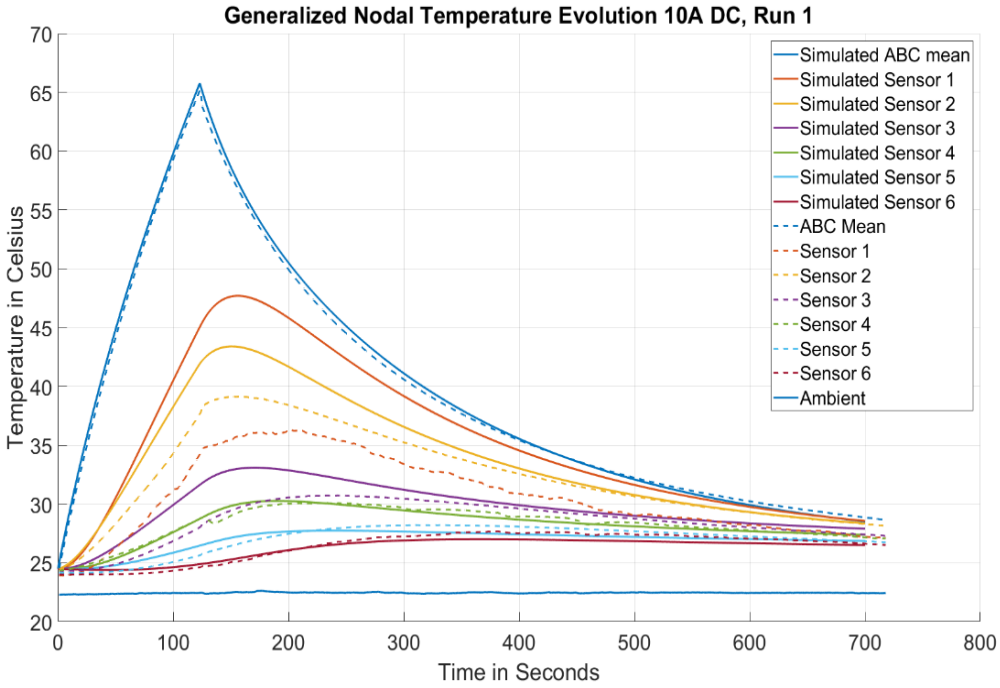

Figure 22: Simulation results for 10A DC, Run 1

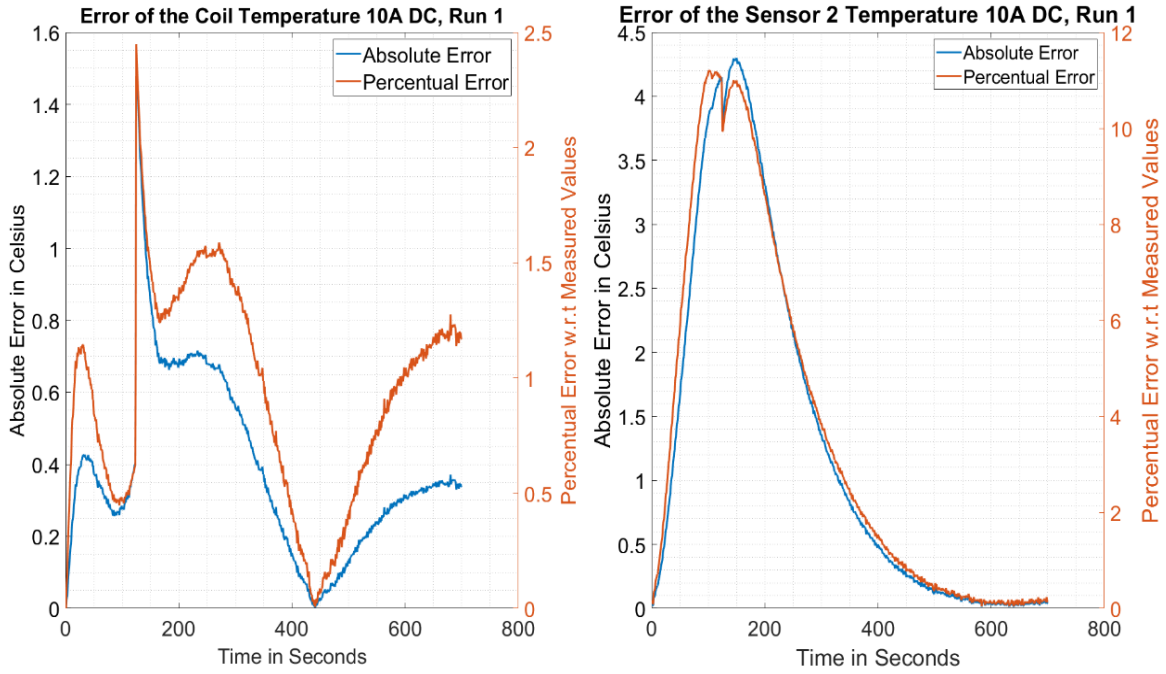

Figure 23: Errors for 10A DC, Run 1

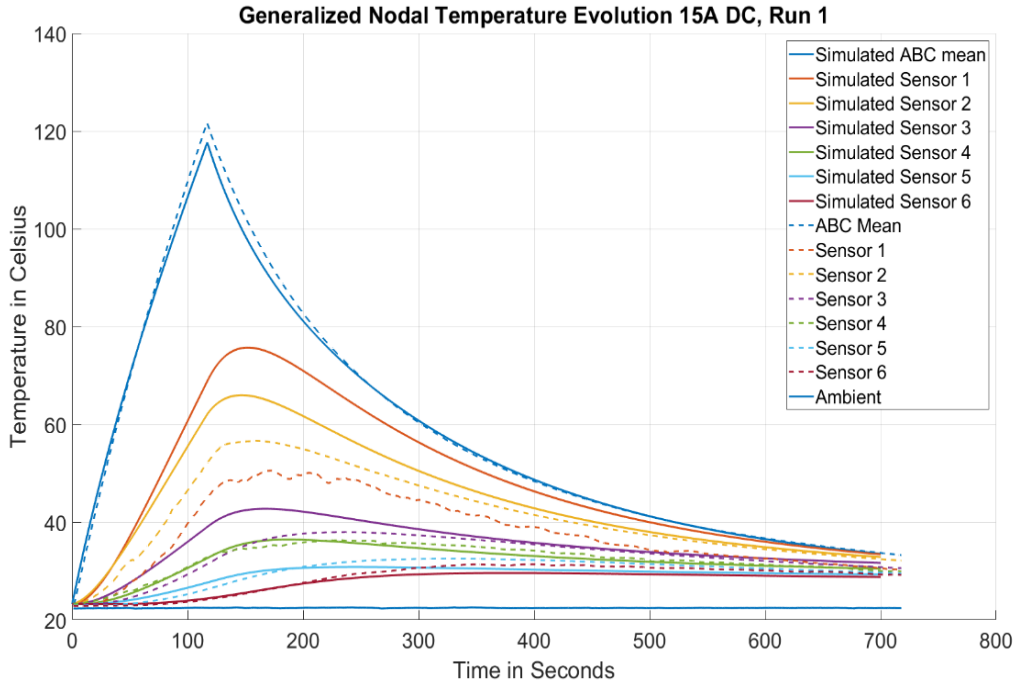

Figure 24: Simulation results for 15A DC, Run 1

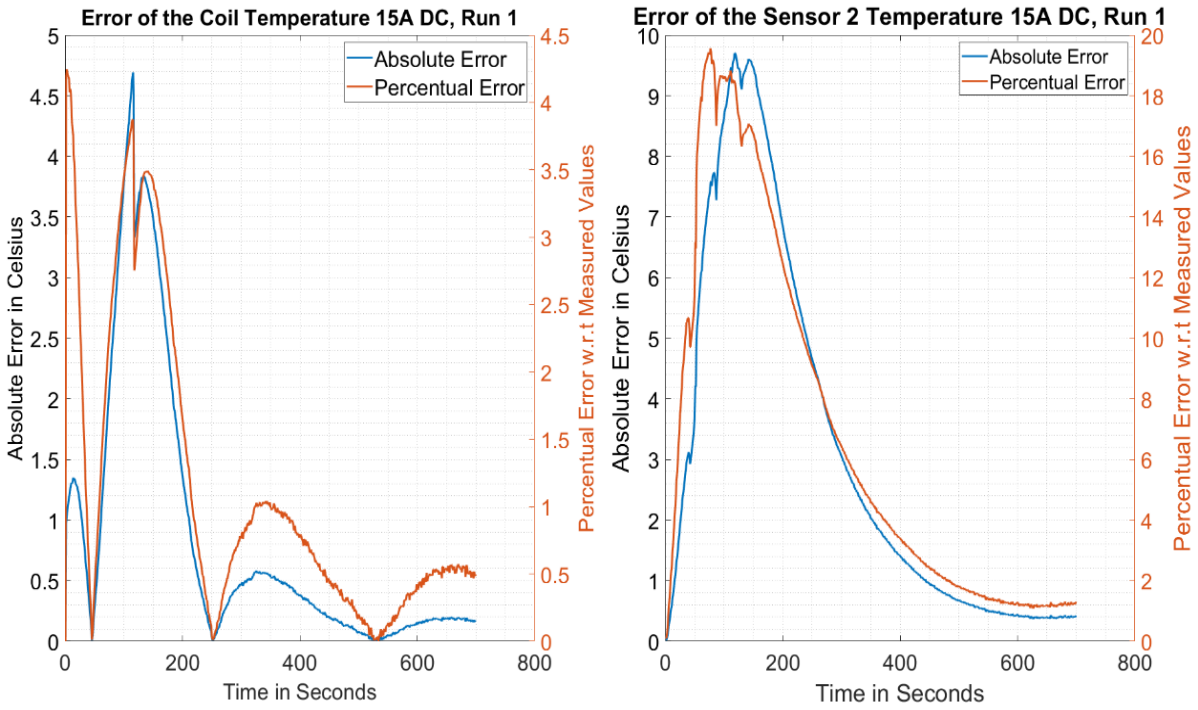

Figure 25: Errors for 15A DC, Run 1

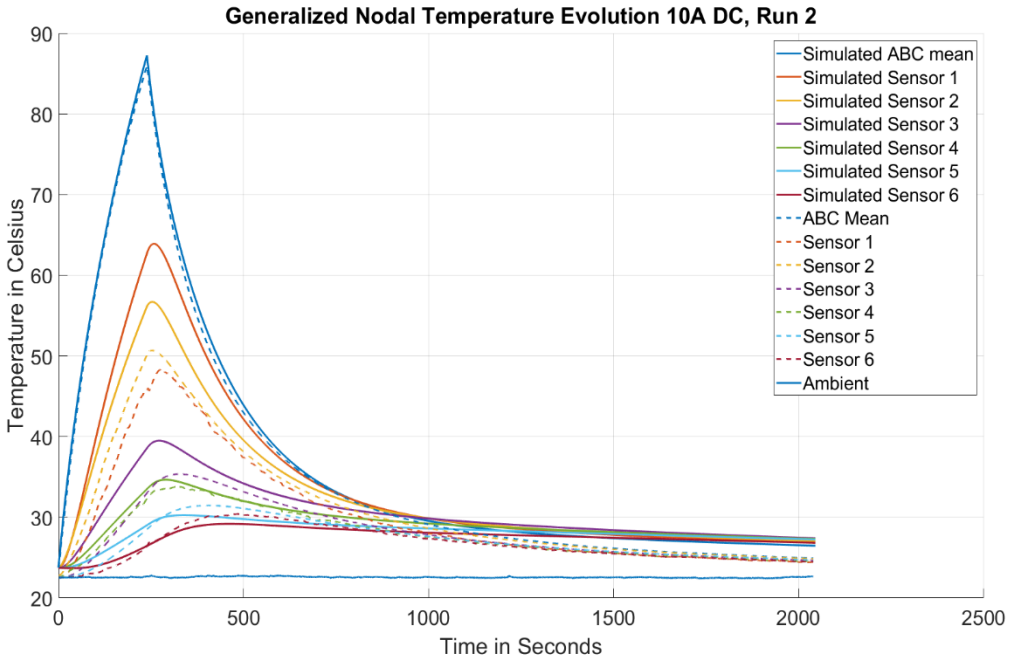

Figure 26: Simulation results for 10A DC, Run 2

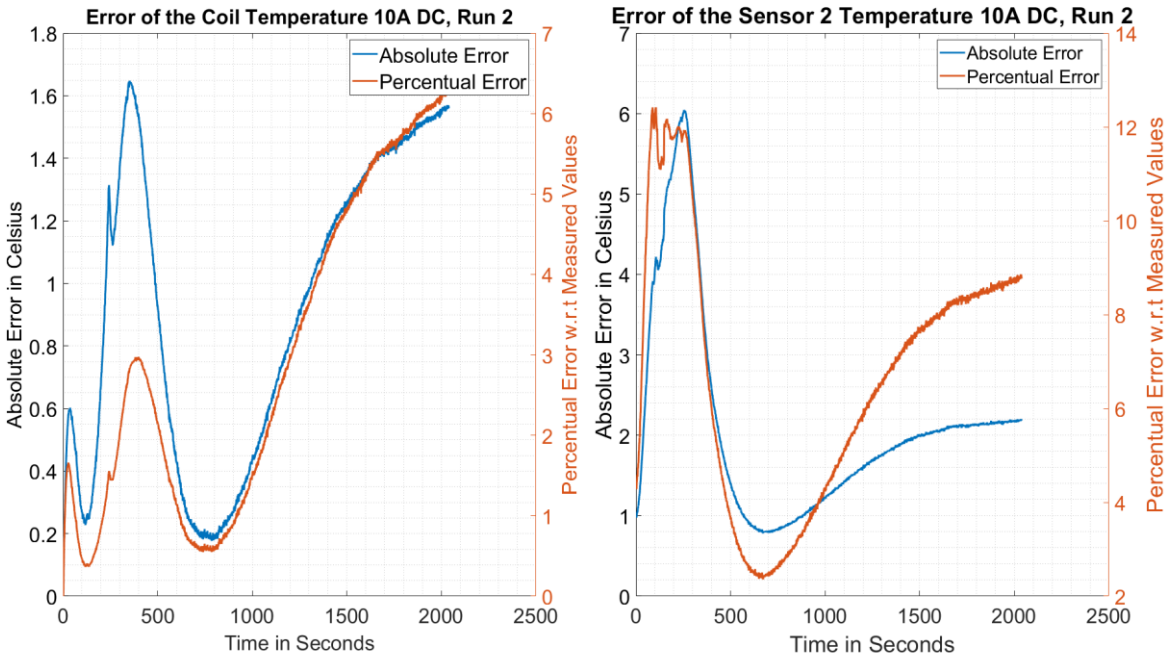

Figure 27: Errors for 10A DC, Run 2

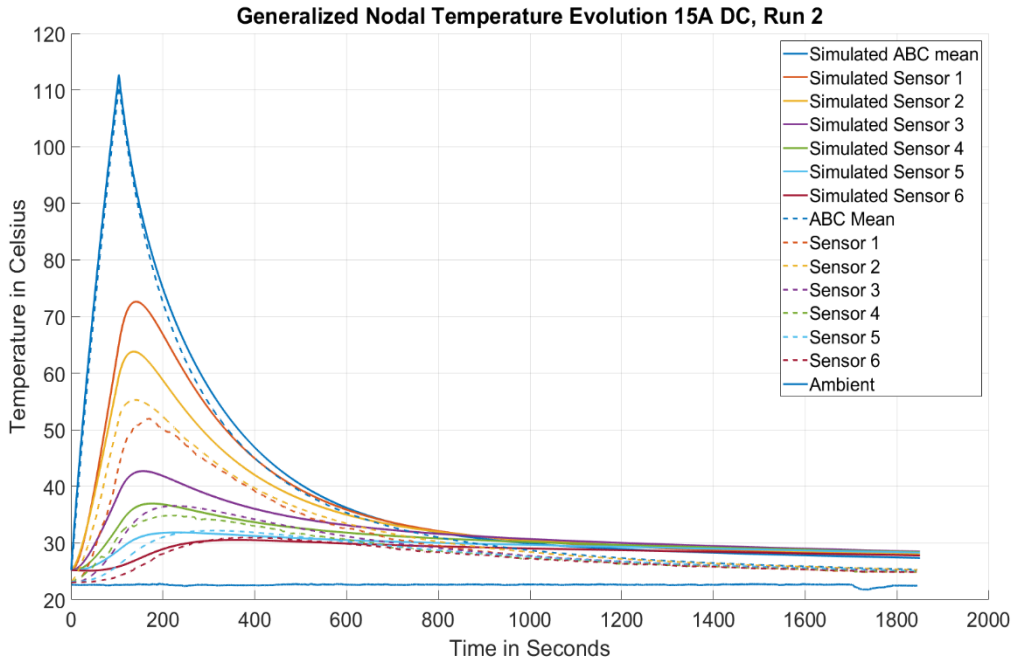

Figure 28: Simulation results for 15A DC, Run 2

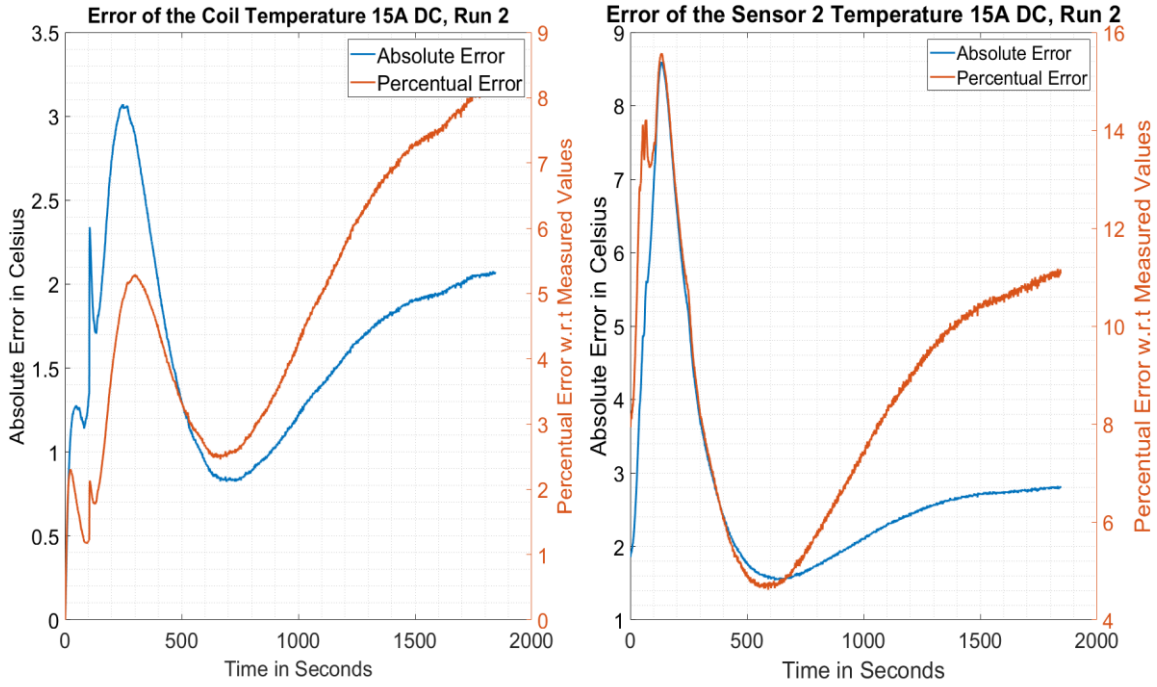

Figure 29: Errors for 15A DC, Run 2

Due to hardware and time constraints the AC tests that were conducted were, by necessity, limited. **Figure 30** depicts a test run with an AC current of 13A RMS at 100Hz, compared to a simple DC simulation. As the available hardware only allowed lower frequencies and the system in question is only a single coil on the stator it was hypothesised that in this condition the AC losses in the coil and the iron losses in the stator would be minimal. That is why the initial comparison of the AC test data was done with respect to a DC simulation, the error of which may be seen in **Figure 31**. After this, the iron losses were implemented into the simulation using the Steinmetz equation and assuming homogenous magnetic flux density throughout the stator along the magnetic path. The results of this and the corresponding errors are depicted in **Figures 32** and **33** respectively.

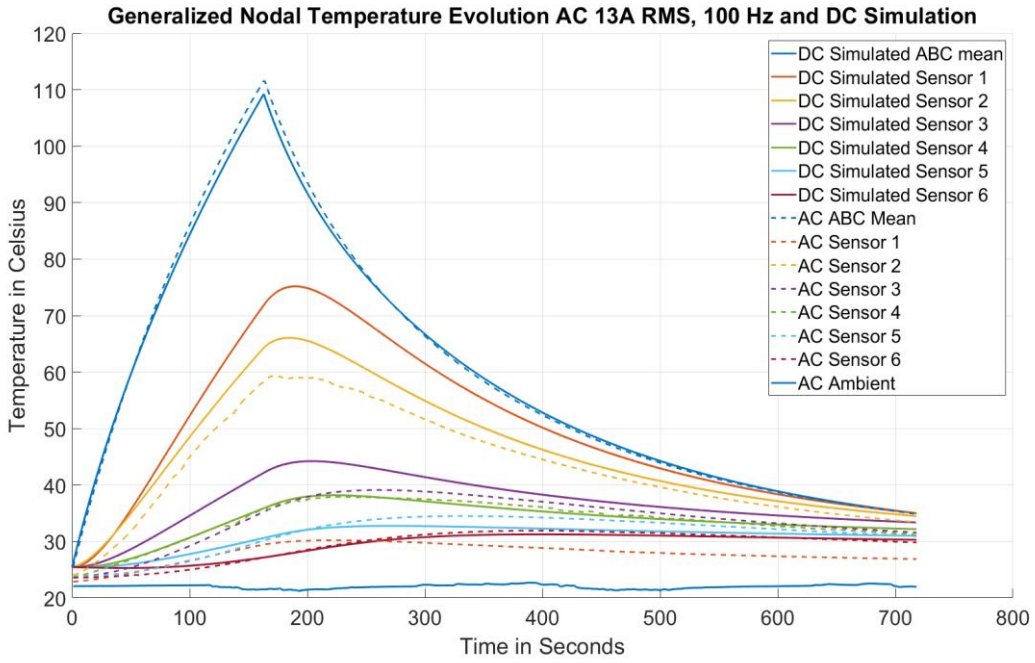

Figure 30: AC test results with DC simulation

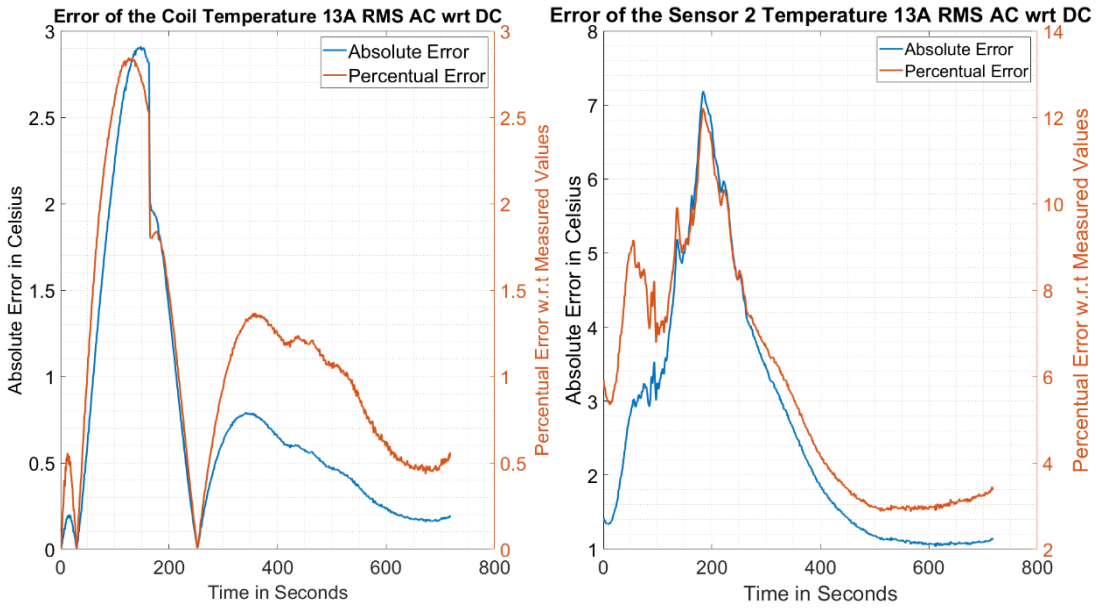

Figure 31: AC tested and DC simulated errors

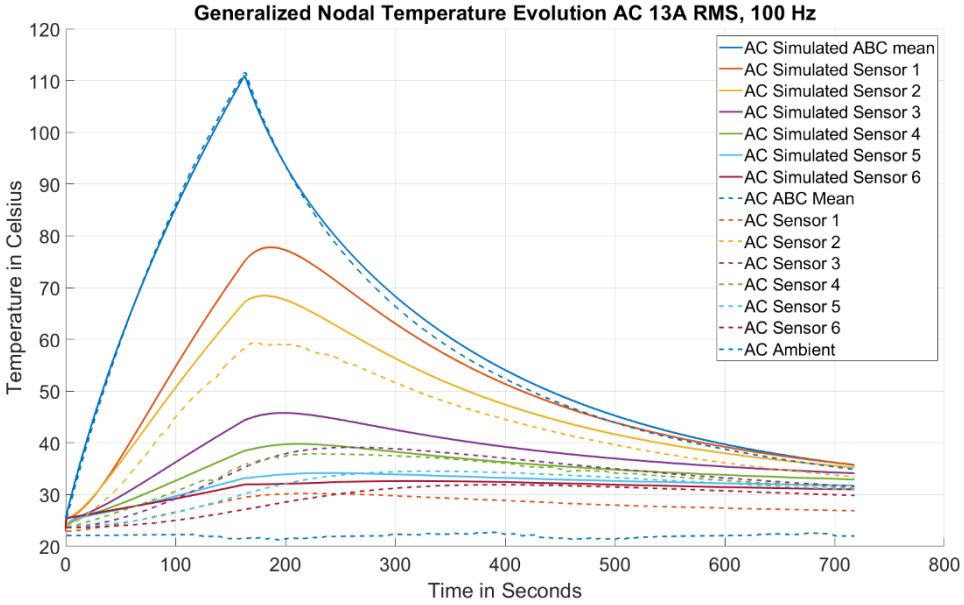

Figure 32: AC test results with AC simulation

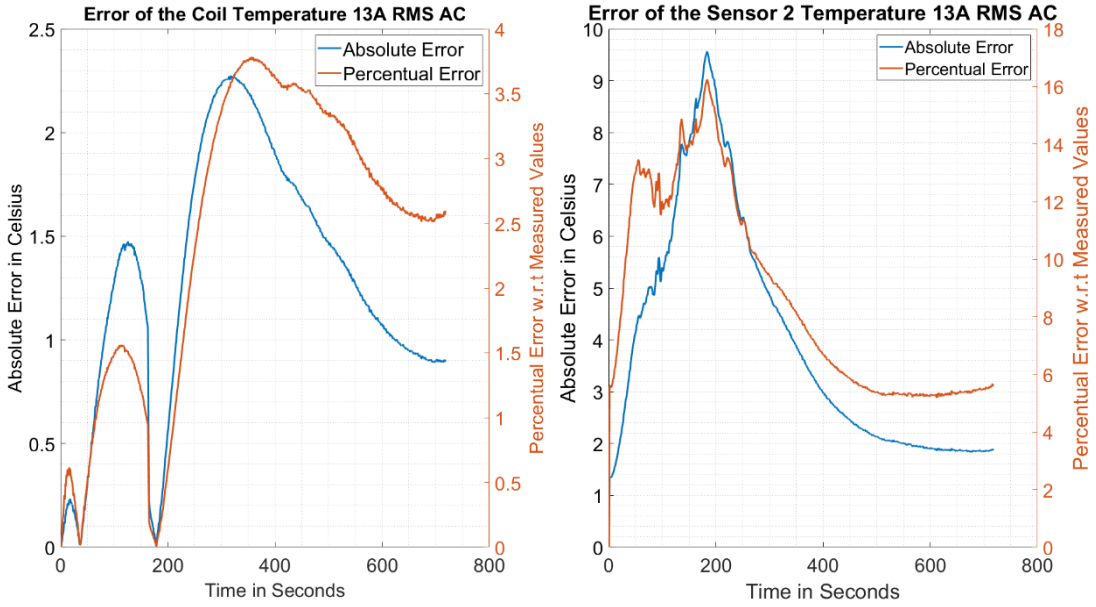

Figure 33: AC tested and simulated errors

It may be observed that during the heating phase the simulation with the implemented iron losses has a marginally smaller error than the DC simulation, from which we can conclude that the method for determining iron losses is accurate. Though the error does get larger towards the end in the cooling phase, however. The cooling error here is the same as previously, which is most likely a results of using a constant h value, rather than a temperature dependant one. Furthermore, the sensor 2 error seems to slightly increase. If we acknowledge the models weaknesses, especially in terms of predicting stator node temperatures, then this result is not unexpected. In DC operations the modelled stator node temperatures already exceed the measured values, and if we now include additional heat sources in the stator nodes from iron losses, it logically follows that the error would slightly increase. More will be said on this point in the discussion and conclusion.

5.4 Second Iteration Discussion

As the reader may have already observed it seems that our second iteration method begins to move in the direction of FEA, which is partially correct. There are, however, a few key distinctions between the model created and conventional FEA software's approach. Firstly, and most importantly the model volumes and areas that are assumed homogeneous are much larger, by orders of magnitude, with respect to regular meshing enacted for FEA. Secondly the heat transfer mechanisms are simplified and laid out in a clearer manner. These two distinctions allow it to become a very powerful tool. Due to its simplicity the solving time of any system becomes very fast, in the range of seconds, whereas FEA may take hours or days to solve complex systems. Additionally, the simplified heat transfer mechanisms allow the user of this algorithm to draw far more direct correlations between real world changes to a system and the resulting thermal behaviour. The cost of this system at the current level is that the calculation of the volumes, distance and surface areas of each node are still done manually, which may be time consuming for larger systems at the beginning. This could be remedied in future work to allow for a more automatic calculation of these values.

Before discussing the overall results' accuracy, we would like to address the possible sources of our errors, which are hypothesised to be fairly numerous, each adding a small amount to the cumulative error. On the hardware side of things, we have identified two main error sources. Firstly, and most importantly, the values of some sensors must be seen sceptically in terms of their accuracy. The actual mounting of the sensors onto the stator was achieved by supergluing them down to the stator material. As the super glue has a certain hardening time, some sensors shifted slightly, meaning they were no longer in direct contact with the metal surface, but engulfed in the glue. This can be seen particularly well in Sensor One during the first run of DC tests, where the temperature data is far from a smooth gradual curve and includes fluctuations. In the second run it was attempted to better attach the sensor, but with limited success. Sensor One does however seem to be giving readings much more similar to those of Sensor Two in the second run, meaning that the correct attachment of sensors is a non-trivial procedure, which can significantly affect result accuracy.

The second hardware source of error would be the actual accuracy of the sensor. Though the global results are quite good, the time step considered in the forward differencing method is extremely small. Over such small increments the accuracy of the thermocouples is far from perfect. This is demonstrated very well in the experimental determinations of the heat transfer coefficients, where the noise of the sensor accuracy is clearly visible.

Lastly on the hardware side of things the actual location of sensor 2 (located between the bobbin and the stator tooth) was hard to determine precisely. The gap between the bobbin and the tooth was very small, leading to the sensor simply being wedged between the two surfaces. The accuracy of determining its location is of course compromised by this fact.

In terms of modelling errors, there were a few simplifications and assumptions made which could lead to additional errors. In all models referred to in this paper the determination of the heat transfer coefficients has been extensively covered, though it has left out the third option of heat transfer. Radiation was deemed to be insignificant for our setup, in a global context, and was hence excluded from the simulation algorithm. Though it is certainly true that compared to convection and conduction the effects of radiation are minimal, they do add to the error to some degree. If this modelling technique is expanded to a full stator or motor configuration, the radiation from one coil to a neighbouring one would most likely no longer be insignificant. It is possible to run the same algorithm, including radiation effects, though a linearisation factor must be experimentally determined, as radiation is not just a function of temperature T but rather of T^4. For further details on this subject **[24]** may considered.

An additional effect leading to disparities is the neglect of thermal contact resistance. The only three locations in the current system where this would be relevant are the heat transfer within the coil from wire to wire, from the coil to the bobbin and from the bobbin to the stator tooth. All these were assumed to have perfect contact and hence no additional thermal resistance. As was shown in the first iteration this assumption is valid to be made for the coil, as the thermal conductance along the wire is good enough to account for it. This is not the case for the coil to bobbin and bobbin to stator tooth contacts. Initially the modelling results did have slightly higher errors. To remedy this a parametric study was conducted to decrease the value of the thermal conductance of the bobbin material. In the electrical analogous circuit what this thermal contact resistance represents is simply another resistor in series with the other ones, meaning that simply increasing the thermal resistance of the bobbin material would have the same effect as finding an equivalent resistance for multiple resistances in series. The manufacturer datasheet of the bobbin stated a heat transfer coefficient k of $0.12 - 0.14 \frac{W}{mK}$. The results of the parametric study concluded that if this value was set to $0.07 \frac{W}{mK}$ instead, the errors were minimised.

In terms of errors in the AC testing a few additional factors must be considered. Due to hardware limitations, it was not possible to ascertain an AC current with a higher frequency than 100Hz and an RMS current of 13A. In these conditions the effects of AC losses in the coil and iron losses in the stator are minimal. In fact, 100Hz results

in a skin depth which is still multiple times the wire diameter, creating a quasi-DC condition inside the coil. The iron losses are however still present, although in a limited capacity, and can be seen in the comparison of the measured AC results with the DC and AC simulations. When comparing the AC and the DC simulations for 13A we can see that all nodes have a slight increase in their temperature and that the stator nodes are also affected by the on and off time of the current in the coil, which is to be expected. The results of adding iron losses into the simulation therefore demonstrate, that the overall error does decrease, except for sensor one which has an extremely large error.

The main reason for the error of sensor one in the AC testing is most likely the additional metal plate attached to the top of the teeth to close the magnetic circuit, which is acting as a heat sink. This extra component was not considered in the simulations. Sensor one was placed on top of the tooth and would therefore be most strongly affected by the effects of the heat sink plate.

Having addressed all the possible sources of errors; the overall result accuracy and its usefulness may now be discussed. When looking at the DC and AC results, we can see that the simulation accuracy is quite high, especially in the heating phase, for both transient and steady state conditions. Though some stator sensor temperatures are overshot by a not insignificant amount the system shows that the coil temperature is modelled extremely accurately. This is of course vital for the safety and longevity of an electric machine as the coils will always be the hottest components, and their insulation class is often the limiting factor in terms of thermal performance. In fact, the results obtained are more accurate than expected and are contrary to the hypothesised ineffectiveness of this method for anisotropic materials which was discussed in **[22].**

The general result of this method of modelling is deemed a success, though further work is still needed. In particular the AC testing was explored in a limited capacity, leaving further research in that direction for future projects. Nevertheless, the overall method and approach strategy has been validated by the experiment results, allowing this methodology to serve as a good foundation which may be expanded upon for more complex systems.

6 Conclusion

This study presented a detailed thermal characterisation and modelling approach for a single-sided axial flux electric motor stator using SMC material. Through a combination of experimental measurements and LPTN modelling, we demonstrated that even a relatively coarse nodalisation strategy can yield accurate and reliable predictions of temperature evolution under both DC and limited AC loading conditions.

Key findings include:

- The use of geometric simplification and rectangular approximations for the coil provides sufficiently accurate results, particularly during heating phases.
- The SMC material exhibits anisotropic thermal conductivity, with significantly lower values compared to pure metals, necessitating accurate experimental parameter identification.
- A multi-node LPTN model, solved numerically via the forward Euler method, successfully captured transient thermal responses across stator regions, with absolute errors consistently under 10 °C and coil temperature errors under 5 °C.
- AC loss modelling using the Steinmetz equation showed promising accuracy, though limited by hardware constraints and the simplified magnetic path.

Despite these successes, the study acknowledges several limitations:

- Thermal contact resistance between coil and stator was neglected and sensor positioning inaccuracies affected data fidelity.
- The simplified AC testing configuration, using a single coil with an external magnetic closure plate, limits generalisability to full motor systems.
- Zero-capacitance or low capacitance nodes should be avoided as much as possible to ensure the stability of the solving algorithm.

Future work should focus on expanding the nodal model to encompass a complete stator, improving material property characterisation (especially for layered or anisotropic systems), and incorporating automated nodalisation from CAD geometries. Furthermore, extending the methodology to include forced convection and real-world duty cycle simulations will enhance its applicability to automotive and aerospace electric machines.

Overall, this work demonstrates a practical, experimentally grounded methodology for thermal analysis that bridges the gap between high-fidelity simulations and scalable design tools—an essential step toward better thermal management in next-generation electric motors.

7 References

[1] B. Bilgin et al., *"Modeling and Analysis of Electric Motors: State-of-the-Art Review,"* in IEEE Transactions on Transportation Electrification, vol. 5, no. 3, pp. 602-617, Sept. 2019, doi: 10.1109/TTE.2019.2931123

[2] L. Shao, R. Navaratne, M. Popescu and G. Liu, *"Design and Construction of Axial-Flux Permanent Magnet Motors for Electric Propulsion Applications—A Review,"* in IEEE Access, vol. 9, pp. 158998-159017, 2021, doi: 10.1109/ACCESS.2021.3131000

[3] K. N. Gyftakis, P. A. Panagiotou, N. Lophitis, D. A. Howey and M. D. McCulloch, *"Breakdown resistance analysis of traction motor winding insulation under thermal ageing,"* 2017 IEEE Energy Conversion Congress and Exposition (ECCE), Cincinnati, OH, USA, 2017, pp. 5819-5825, doi: 10.1109/ECCE.2017.8096964

[4] Emma Arfa Grunditz, *"Design and Assessment of Battery Electric Vehicle Powertrain, with Respect to Performance, Energy Consumption and Electric Motor Thermal Capability"*, Doctoral thesis, Dept. Energy Environ., Chalmers Univ. Technol., Gothenburg, Sweden, 2016.

[5] B. Andersson, *"Lumped parameter thermal modelling of electric machines analysis of an interior permanent magnet synchronous machine for vehicle applications"*, M.S. thesis, Dept. Energy Environ., Chalmers Univ. Technol., Gothenburg, Sweden, 2013.

[6] F. Qi, M. Schenk and R. W. De Doncker, *"Discussing details of lumped parameter thermal modeling in electrical machines,"* 7th IET International Conference on Power Electronics, Machines and Drives (PEMD 2014), Manchester, UK, 2014, pp. 1-6, doi: 10.1049/cp.2014.0479.

[7] A. Boglietti, A. Cavagnino and D. Staton, *"Determination of Critical Parameters in Electrical Machine Thermal Models,"* 2007 IEEE Industry Applications Annual Meeting, New Orleans, LA, USA, 2007, pp. 73-80, doi: 10.1109/07IAS.2007.60.

[8] G. Dajaku and D. Gerling, *"An improved lumped parameter thermal model for electrical machines,"* 2006 17th International Conference on Electrical Machines (ICEM), Chania, Greece, 2006, pp. 1–6. https://citeseerx.ist.psu.edu/document?repid=rep1&type=pdf&doi=66d03357ced40d6cfbaafdbff0e6f140df32f7d9

[9] D. Kuehbacher, A. Kelleter and D. Gerling, *"An improved approach for transient thermal modeling using lumped parameter networks,"* 2013 International Electric Machines & Drives Conference, Chicago, IL, USA, 2013, pp. 824-831, doi: 10.1109/IEMDC.2013.6556188

[10] R. Burke, A. Giedymin, Z. Wu, H. Chuan, N. Bourne and J. G. Hawley, *"A Lumped Parameter Thermal Model for Single-Sided AFPM Machines with Experimental Validation,"* in IEEE Transactions on Transportation Electrification, vol. 6, no. 3, pp. 1065-1083, Sept. 2020, doi: 10.1109/TTE.2020.2998110

[11] A. Boglietti, A. Cavagnino and D. Staton, *"Determination of Critical Parameters in Electrical Machine Thermal Models,"* in IEEE Transactions on Industry Applications, vol. 44, no. 4, pp. 1150-1159, July-aug. 2008, doi: 10.1109/TIA.2008.926233

[12] N. Rostami, M. R. Feyzi, J. Pyrhonen, A. Parviainen and M. Niemela, *"Lumped-Parameter Thermal Model for Axial Flux Permanent Magnet Machines,"* in IEEE Transactions on Magnetics, vol. 49, no. 3, pp. 1178-1184, March 2013, doi: 10.1109/TMAG.2012.2210051

[13] T. L. Bergman, A. S. Lavine, F. P. Incropera, and D. P. DeWitt, *"Fundamentals of Heat and Mass Transfer",* English ed., Loose Leaf, 8th ed. Hoboken, NJ, USA: Wiley, 2020.

[14] J. H. Lienhard V and J. H. Lienhard IV, *"A Heat Transfer Textbook"*, 6th ed. Cambridge, MA, USA: Phlogiston Press, 2024. https://ahtt.mit.edu

[15] A. F. Mills, *"Heat Transfer."* Upper Saddle River, NJ, USA: Pearson Education, 1999.

[16] D. Gerling and G. Dajaku, *"Novel lumped-parameter thermal model for electrical systems,"* 2005 European Conference on Power Electronics and Applications, Dresden, Germany, 2005, pp. 10 pp.-P.10, doi: 10.1109/EPE.2005.219225

[17] J. Shazly, S. Wahsh, and A. Yassin, *"Thermal modeling of an AFPMSM: A review,"* Journal of Electrical Systems and Information Technology, vol. 2, no. 1, pp. 18–26, 2015, doi: 10.1016/j.jesit.2015.03.003

[18] P. H. Mellor, D. Roberts, and D. R. Turner, *"Lumped parameter thermal model for electrical machines of TEFC design,"* Proc. Inst. Electr. Eng. Electr. Power Appl., vol. 138, no. 5, pp. 205–218, Sep. 1991, https://doi.org/10.1049/ip-b.1991.0025

[19] E. Nordlund, S. Tsakok, A. Walker, P. Anpalahan, and M. Lampèrth, *"Lumped circuit thermal model of an axial flux motor,"* in: https://d1wqtxts1xzle7.cloudfront.net/74671806/Lumped_Circuit_Thermal_Model_of_an_Axial20211115-9222-15jpgoy.pdf?1738448964=&response-content-disposition=inline%3B+filename%3DLumped_Circuit_Thermal_Model_of_an_Axial.pdf&Expires=1747859298&Signature=QogyLjP9H0mdDNiF3NIt0Qgz3HR0fg6XBhCNxCWi-S9gChMpTSaEO~8kk6mShUtk4imS8wJTL-ssJ9nFT6M1H9n48Y8BUjSmeP8n2D7DzurByWjtctSrAOn5u2M~BVU-ZfOHeBTW1KbKECEyMTMfJbjG1pL~1tk8VLD4kk4adyI51kooiuLnzYSVW8DGWnw3fd8Uy9bA89~IDd8ijOmgu5G0Tix0KUB4IOR2Op0MNeXy7Sva6XGwp6G6ImJC-UpG2e9XKVkwDpDWbXevCx3~c2Eu-tie8rAEzxtlSBOgEPBnt3f3l4hTKIz0Q4HEHoqrD21XtN1wTv1KcSLyHfXyLA__&Key-Pair-Id=APKAJLOHF5GGSLRBV4ZA

[20] F. Marignetti and V. Delli Colli, *"Thermal Analysis of an Axial Flux Permanent-Magnet Synchronous Machine,"* in IEEE Transactions on Magnetics, vol. 45, no. 7, pp. 2970-2975, July 2009, doi: 10.1109/TMAG.2009.2016415

[21] A. Mohamed, H. Vansompel, A. Hemeida, and P. Sergeant, *"Transient lumped parameter thermal model based loadability studies for the YASA axial flux permanent magnet synchronous machines,"* in Young Researchers Symposium 2018, Brussels, Belgium, Jun. 2018.

[22] V. Lyashenko, E. Kobilskaya and O. Demyanchenko, *"Problems of Mathematical Modeling of Thermal Processes in Electric Machines,"* 2021 IEEE International Conference on Modern Electrical and Energy Systems (MEES), Kremenchuk, Ukraine, 2021, pp. 1-6, doi: 10.1109/MEES52427.2021.9598594

[23] X. Fan, D. Li, R. Qu and C. Wang, *"A Dynamic Multilayer Winding Thermal Model for Electrical Machines With Concentrated Windings,"* in IEEE Transactions on Industrial Electronics, vol. 66, no. 8, pp. 6189-6199, Aug. 2019, doi: 10.1109/TIE.2018.2875634.

[24] Environmental and Thermal Systems Section Applied Mechanics Department, R. McMurchy, R. Payne and R. Dotts, January 1972, *"Thermal Modelling Handbook"*, NASA Contract 9-10435

[25] T. Ishimoto and L. C. Fink, June 1971, *"Systems Improved Numerical Differencing Analyzer"*, NASA Contract 9-10435

[26] A. Engström, C. Johansson, E. Lundgren, E. Klåvus, F. Ekholm, J. Magnusson, T. Höjer, June 2019 Uppsala Universitet: *"Heat transfer in pressed steel powder - Part 1: Temperature measurements in capsules",* ISSN: 1650-8297, 19002 19003

[27] J. P. Holman, 1997, 8th edition, *"Heat Transfer"*, pp. 7, ISBN 0-07-844785-2

[28] Georgia State University, HyperPhysics, 2024 *"Thermal Conductivity"*, in: http://hyperphysics.phy-astr.gsu.edu/hbase/Tables/thrcn.html

[29] GITHUB link to code: https://github.com/James-Keogh/Thermal-Modelling-and-Characterisation-of-an-Axial-FLux-SMC-Stator

[30] R. Roy, S. Ramasami and L. N. Chokkalingam, "Review on Thermal Behavior and Cooling Aspects of Axial Flux Permanent Magnet Motors–A Mechanical Approach," in IEEE Access, vol. 11, pp. 6822-6836, 2023, doi: 10.1109/ACCESS.2023.3235782